Photocopy and Use Authorization

In presenting this thesis in partial fulfillment of the requirements for an advanced degree at Idaho State University, I agree that the library shall make it freely available for inspection. I further state that permission to download and/or print my thesis for scholarly purposes may be granted by the Dean of the Graduate School, Dean of my academic division, or by the University Librarian. It is understood that any copying or publication of this thesis for financial gain shall not be allowed without my written permission.

Signature _____

Date: _____

The design, fabrication, and verification of a solid urethane tissue substitute material to be used in a whole body BOMAB active calibration phantom for In-Vivo counting systems, utilizing gamma ray calibration phantom for In-Vivo counting systems, utilizing gamma ray

by
Michael Thomas Strangfeld

A thesis submitted in partial fulfillment of the requirements for the degree of Master of Science in the Department of Nuclear Engineering and Health Physics

Idaho State University

Fall 2023

To the Graduate Faculty:

The members of the committee appointed to examine the thesis of NAME find it satisfactory and recommend that it be accepted.

NAME,
Major Advisor

NAME,
Committee Member

NAME,
Graduate Faculty Representative

ACKNOWLEDGEMENTS

I would like to acknowledge and express my gratitude to the following individuals and organizations for their support in my research and career development. I would like to thank my major advisor, Dr. Richard Brey, for his commitment to my education, his efforts to enlist me in his program, employment in his lab and for the research opportunities he granted me. I would also like to thank my significant other, family, and friends for their support and consistent belief in me, and the patience they have shown while I developed my career and research. I would like to recognize my late brother who was a pillar of strength in my life, the solid BOMABs decay date is his birthday. He is missed.

I would like to thank my committee members Dr. Rodriguez and Dr. Derryberry. Their commitment to their students is recognized and greatly appreciated. I would like to express my appreciation to Guy Backstrom and the Department of Energy's Radiological Environmental Sciences Laboratory for encouraging and funding my research. Their insight and expertise were invaluable. Finally, I would like to thank the researchers that came before me, we truly do stand on the shoulders of giants.

TABLES OF CONTENTS

List of Figures.....viii

List of Tables.....ix

List of Abbreviations.....xi

ABSTRACT.....xiii

1. Introduction.....1

1.1. Overview.....1

1.2. Problem Statement.....2

1.3. Research Objectives.....2

1.4. Hypothesis Testing.....3

1.5. Structure.....4

2. Literature Review.....6

2.1. BOMAB.....6

2.1.1. History and Uses.....6

2.1.2. ANSI 13.35.....8

2.2. Tissue Equivalency.....11

2.3. Photon Interactions.....12

2.3.1. Photoelectric Effect.....12

2.3.2. Compton Scattering.....13

2.3.3. Pair Production.....13

2.3.4. Effective Atomic Number.....14

2.3.5. Linear Attenuation.....14

2.3.6. Mass Attenuation.....15

2.4. NIST XCOM....16
2.5. Elemental Composistion of Tissues....17
2.5.1. ICRP 23....17
2.6. Irradiated Tissue Determination....19
2.7. Selecting a Tissue Substitute Material....20
2.7.1. Effective Atomic Number Method....21
2.7.2. Elemental Equivalence....23
2.7.3. Basic Data Method....23
2.7.4 Polyurethane....24
2.8. Other Phantoms....25
2.9. ANSI 13.30....26
2.9.1. Relative Bias....26
2.9.2. Relative Precision....27
2.9.3. Root Mean Square Error....28
3. Methodology....29
3.1. In-Vivo Counting System Hardware....29
3.2. Genie 2000 Software....29
3.2.1. Activity....30
3.2.2. Activity Uncertainty....30
3.2.3. Efficiency Development....31
3.2.4. Efficiency Calculation....31
3.2.5. Efficiency Uncertainty....32
3.2.6. Empirical Efficiency Curve....33

3.2.7. Empirical Fit Parameters....34
3.2.8. Empirical Uncertainty....35
3.2.9. Cubic Spline Efficiency....35
3.2.10. Cubic Spline Uncertainty....36
3.2.11. Energy Calibration....36
3.3. BOMAB Criteria....37
3.3.1. Dimension Criteria....37
3.3.2. Volume Criteria....38
3.3.3. Shell Criteria....38
3.4. Tissue Substitute Material Criteria....39
3.4.1. Elemental Equivalence....40
3.4.2. Non-Radiological Criteria....40
3.4.3. Main Component Selection....40
3.4.4. Additive....41
3.4.5. Potassium....42
3.4.6. ^{40}K Activity....43
3.4.7. ^{40}K Verification....44
3.5. Spiking Method....44
3.5.1. Verification of Spiking Method and Homogeneity....45
3.6. Radionuclide Selection and Activity....45
3.7. NIST XCOM Attenuation....47
3.8. BOMAB Fabrication....49
3.8.1. BOMAB Activity and Uncertainty....50

3.9 BOMAB Verification and Calibration.....50

4. Results.....51

4.1. Solid BOMAB Verification.....51

4.2. Solid BOMAB Calibration.....52

4.3. Performance Testing Verification.....56

4.4. Hypothesis Testing.....60

5. Summary and Conclusions.....62

5.1. Summary.....62

5.2. Future Work.....63

6. References.....64

Appendix 1: ANSI 13.30 Minimum Testing Level.....68

Appendix 2: 49 CFR 173.436 Exempt Activity levels.....69

Appendix 3: NIST XCOM Without Additive.....70

LIST OF FIGURES

Figure 2.1: Photographic refence of the BOMAB phantom (ANSI 13.35)….....6

Figure 2.2: Calibration comparison of various phantoms (Schlager 2011)…….8

Figure 2.3: "BOMAB phantom container cross-section. Dimension a is semi minor axis and dimension b is semi-major axis" (ANSI 13.35)….....9

Figure 2.4: The dominant photon interaction based off the energy and atomic number (oncologymedicalphysics.com)….....14

Figure 2.5: The total photon mass attenuation for some material of fixed Z (oncologymedicalphysics.com)….....16

Figure 2.6: The chemical reaction of polyurethane (Gama 2018)….....25

Figure 4.1: V01 empirical curve developed from the solid BOMAB.....52

Figure 4.2: V01 cubic spline curve developed from the solid BOMAB.....53

Figure 4.3: DET10 empirical curve developed from the solid BOMAB.....54

Figure 4.4: DET10 empirical curve developed from the solid BOMAB.....55

Figure 4.5: V01 energy calibration developed from the solid BOMAB.....55

Figure 4.6: DET10 energy calibration developed from the solid BOMAB.....55

LIST OF TABLES

Table 1: The criteria for cross-sectional dimensions and their associated tolerances (ANSI 13.35)….....9

Table 2: Mass attenuation coefficients for ICRU 46 Average soft tissue as listed in ANSI 13.35.....10

Table 3: The tolerance criteria for mass attenuation coefficient and density (ANSI 13.35)…....10

Table 4: Elemental composition of select body components (ICRP 23)….....18

Table 5: Elemental weights in grams for select body tissues (ICRP 23)….....19

Table 6: The elemental composition of the average soft tissue (ICRU 46)….....20

Table 7: Non radiation related criteria for the selection of a tissue substitute material (ICRU 44)….....21

Table 8: The polynomial order to Equation (17), per number of calibration points (Genie 2017)….....34

Table 9: The ANSI 13.35 criteria for cross-sectional dimensions and their associated tolerances compared against measured values.....37

Table 10: The ANSI 13.35 criteria for cross-sectional dimensions and their associated tolerances compared against measured values.....37

Table 11: The ANSI 13.35 criteria for fill volume and their associated tolerances compared against measured values.....38

Table 12: Mass attenuation coefficients for ICRU 46 Average soft tissue as listed in ANSI 13.35 vs NIST XCOM calculated shell mass attenuation coefficients.....39

Table 13: The density criteria comparison of our mixture with the ANSI 13.35 standard.....41

Table 14: Verification results of our potassium salt.....44

Table 15: Verification of the spiking method and its homogeneity.....45
Table 16: The time required to achieve ten thousand counts in the peak area if 5 ml of the standard is taken.....47
Table 17: Chemical formula of the compounds in our mix and their fractional weights.....48
Table 18: NIST XCOM's calculated attenuation for the tissue substitute with additive compared to the coefficients defined in ANSI 13.35.....48
Table 19: BOMABs fractional percentage per volume based on ANSI 13.35.....49
Table 20: BOMAB calculated activity and uncertainty.....50
Table 21: Verification results for Solid BOMAB.....51
Table 22: The deviation of the V01 empirical curve as calculated by Genie.....53
Table 23: The deviation of the DET10 empirical curve as calculated by Genie.....54
Table 24: Performance Testing BOMAB verification using an empirical curve on V01.....57
Table 25: Performance Testing BOMAB verification using a cubic spline curve on V01.....58
Table 26: Performance Testing BOMAB verification using an empirical curve on DET10.....59
Table 27: Performance Testing BOMAB verification using a cubic spline curve on DET10.....60
Table 28: ANSI 13.30's minimum testing levels for direct radiobioassay.....68
Table 29: Exempt activity levels, per radionuclide, listed in 49 CFR 173.436.....69
Table 30: NIST XCOM's calculated attenuation for our tissue substitute without additive compared to the coefficients defined in ANSI 13.35.....70

LIST OF ABBREVIATIONS

^{134}Cs	Radioactive isotope of cesium
^{137}Cs	Radioactive isotope of cesium
^{152}Eu	Radioactive isotope of europium
^{40}K	Radioactive isotope of potassium
^{54}Mn	Radioactive isotope of manganese
^{60}Co	Radioactive isotope of cobalt
ANSI	American National Standards Institute
Avg	Average
BOMAB	Bottle Manakin Absorption Phantom
BR	Branching Ratio
C	Carbon
CFR	Code of Federal Regulations
Ch	Channel
cm	centimeter
DET10	small diameter, low efficiency detector, cooled with an X-cooler III
DOE	Department of Energy
DOELAP	Department of Energy Laboratory Accredidation Program
eff	Efficiency
FWHM	Full width at half maximum
g	gram
GPS	Gammas per second
H	Hydrogen
HPS	Health Physics Society
ICRP	International Commission on Radiological Protection
ICRU	International Commission on Radiation Units and Measurements
IEC	International Electrotechnical Commission

INL	Idaho National Laboratory
ISO	International Organization for Standardization
K_2CO_3	Potassium carbonate
keV	Kiloelectron volt
MCA	Multi-channel analyzer
MDA	Minimum detectable activity
MeV	Megaelectron volt
MIRD	Medical Internal Radiation Dose
ml	Milliliter
N	Nitrogen
nCi	Nanocurie
NIST	National Institute of Standards and Technology
O	Oxygen
pCi	Picocurie
RANDO	Anthropomorphic phantom developed by Alderson
RESL	Radiological and Environmental Sciences Laboratory
RMSE	Root mean squared error
s	Seconds
stdev	Standard deviation
tot	Total
V01	Large diameter, high efficiency detector, cooled with an ICS-P4 cooling system
w/v	Weight in Volume
XCOM	Photon Cross Sections Database
Z	Atomic Number

The design, fabrication, and verification of a solid urethane tissue substitute material to be used in a whole body BOMAB active calibration phantom for In-Vivo counting systems, utilizing gamma ray spectroscopy.

Thesis Abstract—Idaho State University 2023

Since the discovery of x-rays, tissue substitute materials have been developed to aid in the investigation of irradiated tissues and improvement of diagnostic and therapeutic techniques. This research continues to explore their development with the fabrication of a solid tissue substitute material that simulates soft tissue. In this effort the soft tissue substitute defined in ICRU 46, was used as a filler material in a calibration BOMAB (Bottle Manakin Absorption Phantom) for In-Vivo counting systems. This type of phantom has utility during the calibration of gamma ray spectroscopy systems integral to in-vivo bioassay.

Our tissue design was developed using guidance from ICRU 44, ICRU 46 and (Griffith 1980) research into polyurethane. The tissue substitute was made from commercially available materials, does not require unique laboratory equipment and can be modified to simulate different tissue types based on the ratio of our mixture and selective additives. A solid BOMAB offers significant advantages that resolve shipping hazards and leaking that arise from the use of aqueous filled phantoms, as well as the benefits of trapping off-gas in long lived natural chains, like radium, creating a calibration source in equilibrium that would outlive generations to come.

The solid BOMAB was built using guidance from RESLs BOMAB procedure and ANSI 13.35. The concentration of radioactive material and its distribution in the solid BOMAB was developed using guidance from ANSI 13.30 and 49 CFR 173.436. The radionuclide ^{152}Eu was used because it has a sufficient number of energy lines to create a multipoint calibration curve and based on the RESL development an adequate activity to minimize counting times. The solid

BOMAB was verified against a NIST traceable aqueous filled BOMAB with the same radioactive material. The measured radioactivity in the solid BOMAB was found to be within 1% of its calculated spike activity at the 121, 344, 1112 and 1407 keV peaks. The In-Vivo counting system consists of two aluminum capped high purity germanium detectors, having 30% and 100% relative efficiency. This analysis was completed inside a vault made from pre-World War II steel, to minimize background interference.

After calibrating the In-Vivo counting system with the solid BOMAB, empirical and cubic spline efficiency curves were developed and employed in the verification of a DOELAP performance testing BOMAB. It was found that these efficiency curves developed from the solid BOMAB calibration effort were able to verify the performance testing BOMAB based on the criteria set forth in ANSI 13.30. Therefore, this effort verified the tissue substitute for use in wide ranging applications and may serve as an adequate replacement for aqueous filled BOMABs for calibration and performance testing.

Key words: tissue substitute, BOMAB, In-Vivo, gamma ray spectroscopy.

1. INTRODUCTION

The protection and monitoring of workers and the public from internal and external exposures from sources catastrophically large or seemingly insignificant require the use of phantoms. A phantom can be as simple as water and wax in a cubic geometry or as complicated as voxel phantoms that require Monte Carlo simulation. All phantoms, even simple geometrical phantoms, are filled with material that simulate the radiation properties of the tissues they represent. It is the scope of this research to develop a material that simulates soft tissue, to be used in a BOMAB phantom. A solid BOMAB offers significant advantages that resolve shipping hazards and leaking that arise from the use of aqueous filled phantoms, as well as the benefits of trapping off-gas in long lived natural chains, like radium, creating a calibration source in equilibrium that would outlive generations to come.

1.1 Overview

Bottle Manakin Absorption Phantom, BOMAB, is a representation of the human body made up of seven right angle circular cylinders (legs, thighs, arms, and neck) and three elliptical cylinders (hip, chest, and head). The shells are made with a tissue substitute material, typically polyethylene and the circular cylinders are filled with radioactive water solutions. This anthropomorphic model is used to simulate average soft tissue for photon interactions for energies ranging from 100 keV to 3 MeV (ANSI 13.35).

BOMABs are used for a variety of applications: the determination of background, MDA, counting efficiencies, activity distribution dependence, size dependence, precision of a counting system, performance testing, calibration and radiotherapy (ANSI 13.35). Similarly, tissue substitute materials are commonly used in the estimation of absorbed dose, detector materials as

well as radiotherapy, radiodiagnosis, radiation protection and radiobiology (ICRU 46). This present effort combines these two concepts by using solid plastics with equivalent radiation properties as a solid radioactive filler. This combination constitutes an anthropomorphic phantom.

1.2 Problem Statement

The current system of developing calibration and performance testing standards uses water as a fill material. A water filled BOMAB tends to leak, especially when undergoing pressure differences during overnight air shipments - their primary mode of transport. To keep radionuclides in solution usually requires acidic conditions, this adds additional hazardous and shipping concerns. Consistently, special storage and handling protocols are needed to avoid evaporation or catastrophic failure of the shell.

Other research has sought to eradicate the problems associated with aqueous fillers and developed BOMABs filled with tissue substitute material. Unfortunately, much of this work has been lost to the retirement of previous generations. Some records and procedures remain, but show batch process, anti-foaming agents, valves, vacuum systems, obsolete chemical mixtures and large mixers (LLNL 2023). This is a tedious and arduous process which should and can be simplified.

1.3 Research Objectives

It is the fundamental objective of this thesis to design, fabricate and verify a BOMAB phantom filled with a solid urethane tissue substitute material made from commercially available materials, in a less burdensome manner than previous approaches and to eliminate recurring problems of the current methods. By so doing, this effort will contribute to the advancement of

radiation protection and dosimetry by providing a reliable and accurate phantom used for calibration, as well as a modifiable tissue substitute material that can be used for a wide variety of applications.

1.4 Hypothesis Testing

First: Solid BOMAB compared to NIST traceable aqueous BOMAB

Alternative: The activity derived from the genie software will not be statistically identical to the calculated spike activity

Null: The activity derived from the genie software will be statistically identical to the calculated spike activity, verifying it as a tissue substitute by comparison

We will test this by analyzing the solid BOMAB spectra using the energy and cubic spline interpolated efficiency calibration from a NIST traceable aqueous filled BOMAB that uses the same radionuclide(s). The derived activity will be deemed to be statistically identical if its value is found to be within two standard deviations of its known value.

Second: Solid BOMAB compared to DOELAPs Performance Testing BOMABs

Alternative: The calibration curves developed from our fabricated BOMAB will not verify the performance testing BOMAB

Null: The calibration curves developed from our fabricated BOMAB will verify the performance testing BOMAB

We will test this by analyzing the spectra of the performance testing BOMAB using the energy and efficiency calibration from the solid BOMAB. The performance testing BOMAB is verified per the statistical analysis criteria set forth in ANSI 13.30, namely using the mean relative bias and relative precision to calculate the root mean squared error.

1.5 Structure

This thesis is structured into 6 sections and 3 appendices. The current section is the introduction where a quick overview, problem statements, research objectives and hypotheses are given. The second section is the literature review which discuss the history and uses of the BOMAB phantom, the criteria and guidance on its current fabrication, the history of tissue substitute material and the photon interactions within that medium, the composition of the irradiated tissue, the guidance and criteria for the development of a tissue substitute material, polyurethane, and the statistical analysis use in radiobiassay performance testing. The third section covers the methodology of our research, the In-Vivo counting system hardware and software including calculated values and efficiencies, the fabrication of the solid BOMAB, the selection and development of the tissue substitute its additives and background, the selection of radionuclide and associated activity, and attenuation coefficients. The fourth section is the results, the verification of the solid BOMAB, its use as a calibration standard, the verification of a performance testing BOMAB using ANSI 13.30 statistical analysis, and hypothesis testing. The fifth section is our summary, and the future work. The sixth section, the references, is proceeded by 3 appendices.

2. LITERATURE REVIEW

2.1 Bottle Manakin Absorption Phantom, BOMAB

2.1.1 History and Uses

BOMABS are an early anthropomorphic phantom used in a variety of radiological applications but are primarily used in radiation protection as a calibration standard for In-Vivo counting systems, specifically for the measurement of the whole body distributed of radionuclides such as ^{137}Cs or ^{40}K (ANSI 13.35).

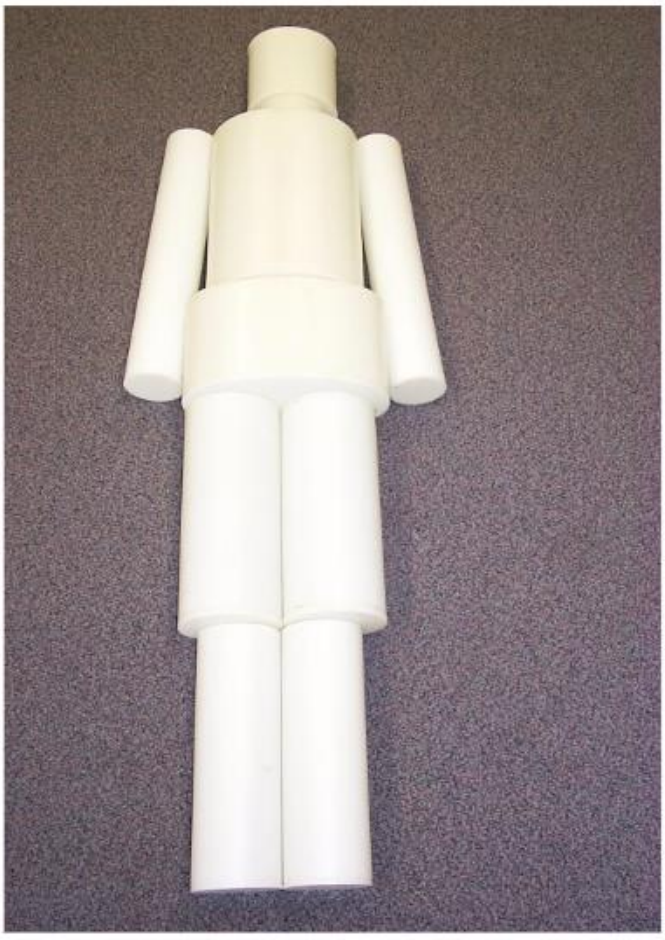

Figure 2.1: Photographic refence of the BOMAB phantom (ANSI 13.35).

Early BOMABs were empty shells containing a "core of air" and were used in radium therapy to determine the integral dose of a model patient. Bush positioned a radium point source in 800 different positions to calculate the energy absorption (Bush 1946). Bush continued his calculation of integral dose with a BOMAB phantom filled with a "uniformly distributed gamma-ray emitting radioactive [material]" (Bush 1949). Nuclear power applications also used BOMABs to analyze the amount of activated sodium from a neutron source or after a criticality event (Sanders 1962; Delafield 1974).

BOMABs are used for a variety of other applications: The determination of background, MDA, counting efficiencies, activity distribution dependence, size dependence and precision of a counting system, calibration, and radiotherapy as well as performance testing (ANSI 13.35). BOMABs are an active calibration standard and have also been used in comparative studies.

More recently, "analysis was performed by means of Monte Carlo simulations with the Monte Carlo N-Particle transport code using detailed mathematical models of the phantoms (…). The simulated peak efficiencies for the BOMAB phantom and the MIRD phantom agree very well" (Schläger 2011). Figure 2.2 seen below depicts a comparison of the efficiency curves for the MIRD model, the BOMAB labeled RMB, and the St. Petersburg block phantom, a phantom similar in overall structure to the BOMAB, but uses modular solid polyethylene blocks.

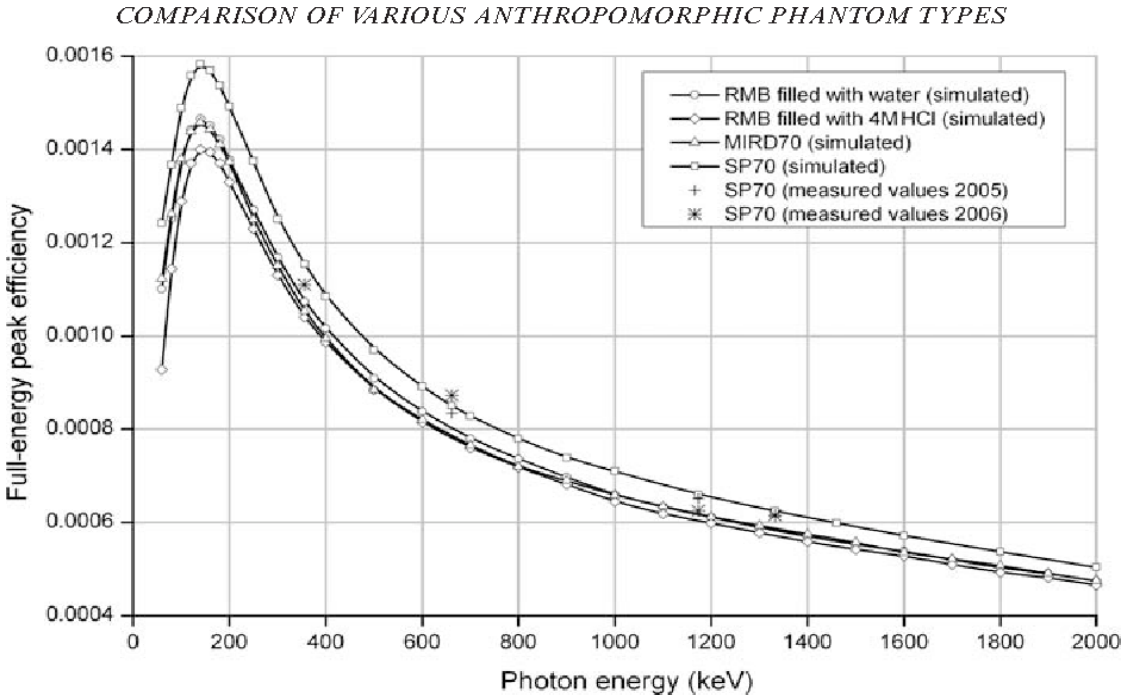

Figure 2.2: Calibration comparison of various phantoms (Schlager 2011).

Furthermore, "In practice, computational models (…) are frequently used to define the physical quantities that have to be determined in the specification of dose equivalent, which generally cannot be measured directly. Calibration phantoms are then fabricated for the calibration of the measurement systems (in-vivo counters, dosimeters, etc.) that are employed to determine these physical quantities" (ICRU 48).

2.1.2 Development and ANSI 13.35

The American National Standard Institute, ANSI, HPS 13.35, developed by the Health Physics Society is a standard that "establishes the specifications for the design and fabrication of bottle manikin absorption (BOMAB) phantoms". This standard does not give specific instructions for the fabrication but does provide guidance in the criteria of their design (ANSI 13.35).

The first criteria are the physical specifications, namely the outside cross-sectional dimensions for each bottle shall meet tolerances. Figure 2.3 below shows the labeled dimensions of the cross section of the BOMAB. Table 1 below shows the dimension criteria, developed from Bush circa 1946, and their tolerances (ANSI 13.35).

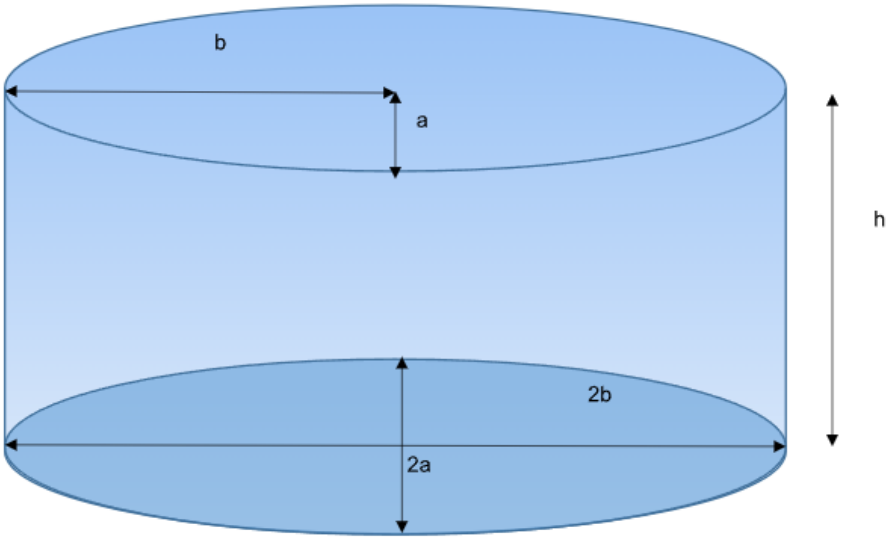

Figure 2.3: "BOMAB phantom container cross-section. Dimension a is semi minor axis and dimension b is semi-major axis" (ANSI 13.35).

Table 1: The criteria for cross-sectional dimensions and their associated tolerances (ANSI 13.35).

Section	Dimension 2a (cm) +/- 5%	Dimension 2b (cm) +/- 5%	Height h (cm) +/- 5%	Fill Volume (cc) +/- 18%	Thickness (cm) +/- 10%
Head	14	19	20	3490	0.5
Neck	13	13	10	1020	0.5
Thorax	20	30	40	16900	0.5
Abdomen	20	36	20	9920	0.5
Thighs	15	15	40	6000	0.5
Calves	12	12	40	3710	0.5
Arms	10	10	60	3750	0.5
Total			170*	58200**	

*: Total Height does not include arm measurements.
**: Total Fill Volume includes twice the value of arms, thighs and calves.

The second criterion is specifications on the material composition. The BOMAB shall have a shell and a filler material of tissue substitute material that simulate the radiation interaction properties at energies between 100 keV and 3 MeV of average soft tissue as defined by ICRU 46 (ANIS 13.35). Table 2 and Table 3 seen below show the criteria for radiation interaction properties and the tolerance criteria for material composition respectively.

Table 2: Mass attenuation coefficients for ICRU 46 Average soft tissue as listed in ANSI 13.35.

Photon Energy (MeV)	Mass Attenuation Coefficient (m^2/kg)
0.1	0.01690
0.2	0.01360
0.5	0.00960
1.0	0.00700
1.5	0.00570
2.0	0.00490
2.5	0.00430
3.0	0.00393

Table 3: The tolerance criteria for mass attenuation coefficient and density (ANSI 13.35).

Section	Mass Attenuation Coefficient*	Density (kg/m^3)
Filler	+/- 5%	1005 +/- 5%
Shell	+/- 10%	950 +/- 5%

* Values are shown in Table 2.

Further criteria for the BOMAB are the filler materials shall be "chemically compatible" with the shell, and the shell shall have physical integrity to avoid leaking. The density and activity of the phantom shall be determined quantitatively, and the activity will be homogenous in each section and NIST traceable. The uncertainty of the activity and subsequent verification will include the uncertainty of the spiking standard, dilution volume, gravimetric measurements and counting statistics. Finally, "potassium can be incorporated into the phantom for

applications such as estimating MDA values or estimation background count rates" (ANSI 13.35).

2.2 Tissue Equivalency

The current system of monitoring workers and the public requires phantoms, like the BOMAB, to help assess exposure and quantify absorbed dose estimations to specific organs or whole body (ICRP 110). Phantoms are a physical geometry the simulates parts of the human body (ANSI 13.35). An active phantom is filled with radionuclides imitating internal depositions (IRCU 48). These phantoms are used primarily for calibration, determining MDA, background estimates, and quality assurance testing. Some of the most common phantoms seen in any In-Vivo program are lungs, thyroid, whole body RMC-II phantoms and their inserts simulating localized radioactivity, liver and BOMAB.

Phantoms simulate more than just the geometry of the human body. Their filler material also mimics the radiation attenuation properties of the target irradiation tissues for specific energy ranges. This phenomenon was referred to as tissue equivalency and was first introduced by (Kienböck 1906) to replicate irradiated tissues from diagnostic techniques like x-ray. Early reports of ICRU, namely 10d, 24, and 30 continued to refine this concept. The term equivalency, in the past, was used erroneously to mean simply providing characterization of a material by its attenuation properties. This explicitly is no longer considered sufficient to classify a material as equivalent to tissue. Instead, the term tissue substitute is now the common nomenclature used to avoid confusion (ICRU 44). ICRU 30 defines tissue equivalent material as "a material, the absorption and scattering properties of which, for a given irradiation, simulate as nearly as possible those of a given biological material".

2.3 Photon Interaction

Photons interact with tissue substitute materials in three main ways: the Photoelectric effect, Compton scattering, and Pair production. Each interaction has dependencies on the photon energy, the atomic number of the absorber and is governed statistically by its probability (Martin 2013).

2.3.1 Photoelectric Effect

The photoelectric effect is an interaction involving a photon and a tightly bound electron. If the energy of the incident photon is equal to or greater than the binding energy of the electron, then the energy of the photon is absorbed by the atom and the process of ionization occurs. Ionization is the ejection of the bound electron. This newly ejected electron, known as a photoelectron, continues to excite and further ionize along its trajectory dependent on its energy. The rough approximation for the probability of this type of interaction is seen below in Equation (1) (Martin 2013):

$$\sigma_F = (Z^n / E^3) \qquad \text{Eq. (1)}$$

Where:

σ_F = Photoelectric probability

Z = atomic number of the material

n = "an exponent with a value between 4 and 5 over the gamma ray energy region of usual interest"

E = incident photon energy

2.3.2 Compton Scattering

Compton scattering is an elastic collision, where momentum is conserved, between a "free" electron and the incident photon. A free electron is an electron whose binding energy is considerably less than the incident photon. This scattered electron, known as the Compton electron, continues to excite and further ionize along its trajectory dependent on its energy. The rough approximation for the probability of this type of interaction is seen below in Equation (2) (Martin 2013):

$$\sigma_C = (Z / E) \qquad \text{Eq. (2)}$$

2.3.3 Pair Production

Although photoelectric effect and Compton scattering predominate from the energy range of 0.5 to 5 MeV, there is a third type of interaction that begins at 1.02 MeV, pair production. In pair production, the full absorption of the photon is followed by the creation of a positron-negatron pair. The sum of these particles has the same energy as the incident photon and move in opposite directions from each other to conserve momentum. The rough approximation for the probability of this type of interaction is seen below in Equation (3) (Martin 2013):

$$\sigma_P = Z^2 * (E\text{-}1.02) \qquad \text{Eq. (3)}$$

As seen above, the probability of these interactions is energy dependent and proportional to the atomic number of the material. As one or both variables change, the type of interaction

becomes more or less likely. Figure 2.4, seen below, is a graphic representation of the probabilities of photon interaction dependency on the atomic number at specific energies (oncologymedicalphysics.com).

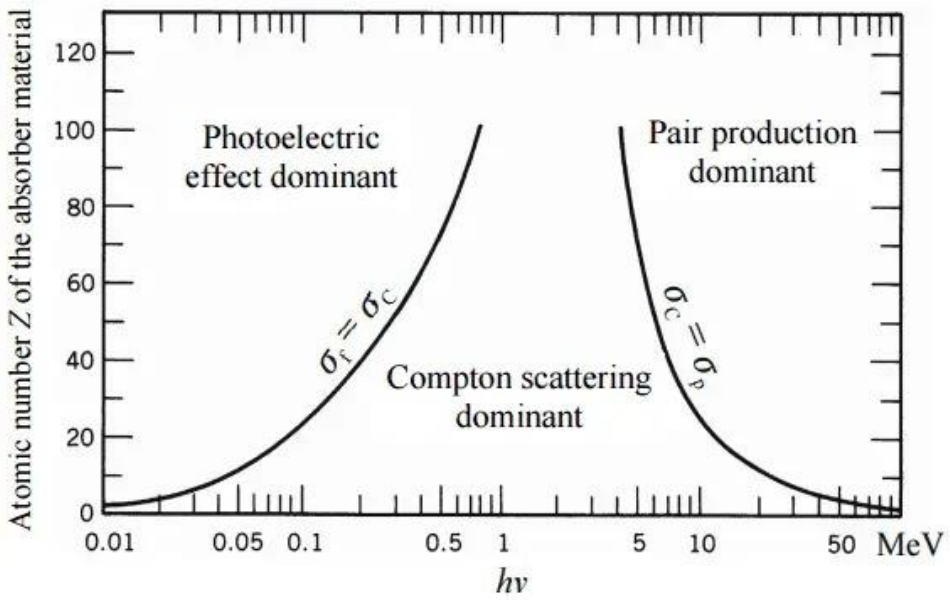

Figure 2.4: The dominant photon interaction based off the energy and atomic number (oncologymedicalphysics.com).

2.3.4 Effective Atomic Number

A near homogeneous mixture of different elements with different atomic numbers will have a new atomic number that represents the composite, defined as the effective atomic number, Z_{eff}. Effective Z is discussed further in Section 2.7.1.

2.3.5 Linear Attenuation

As photons traverse a medium, they interact through scattering and absorption. These interactions decrease the intensity of the incident beam, as seen in Equation (4). This is the process of attenuation. The probability of penetration is best expressed through the idea of the

linear attenuation coefficient. The linear attenuation coefficient is the probability a photon experiences an interaction while traveling some distance through a material (Martin 2013).

$$I = I_o * e^{-\mu x} \qquad \text{Eq. (4)}$$

Where:

I = final photon beam intensity

I_0 = incident photon beam intensity

μ = linear attenuation coefficient

x = distance traveled

2.3.6 Mass Attenuation

The analysis of the probability of attenuation through a material with known density is known as mass attenuation. "The total mass attenuation coefficient may be expressed as the sum of its [probability] components" at a particular energy. This relationship can be seen below in Equation (5) (ICRU 44).

$$(\mu/\rho) = (\sigma_f/\rho) + (\sigma_C/\rho) + (\sigma_P/\rho) \qquad \text{Eq. (5)}$$

Where:

ρ = density of the absorber material

A graphic representation of the mass attenuation coefficient can be seen below in Figure 2.5 (oncologymedicalphysics.com).

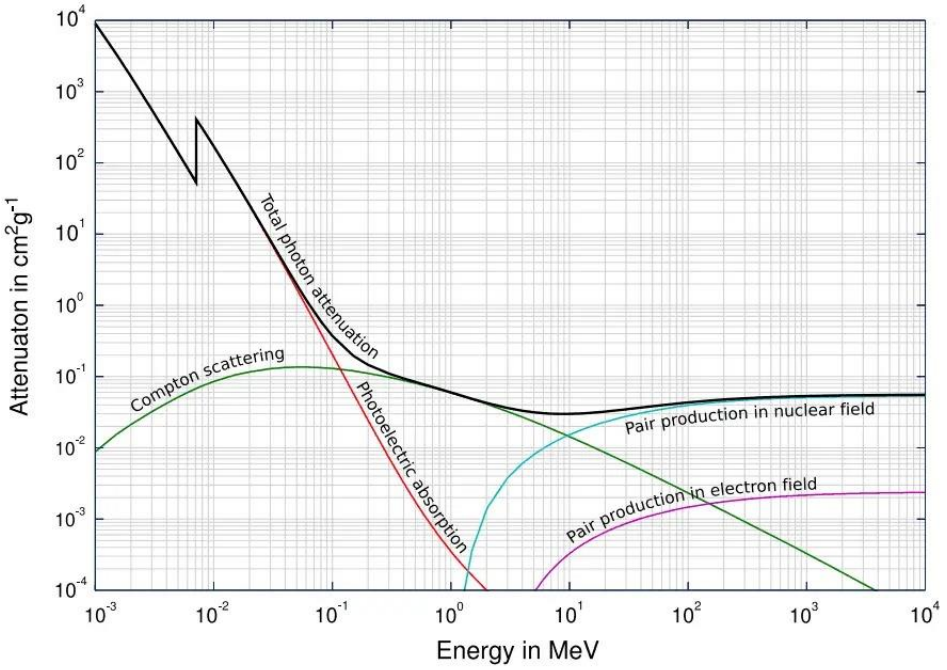

Figure 2.5: The total photon mass attenuation for some material of fixed Z (oncologymedicalphysics.com).

2.4 NIST XCOM

Mass attenuation coefficients can be determined empirically or by employing interpolation from known values in the many available tables found in the literature. The National Institute of Science and Technology has a database software application that can perform those calculations for a user so long as they know the chemical formula of each compound in the mixture, and the elemental fractional weights. NIST XCOM employs a cubic spline fit approximation as a function of energy (NIST XCOM). Section 3.2.9 goes into further detail of cubic spline fitting.

NIST XCOM is considered by many to be an authoritative database and is used by ANSI and ICRU. The advantages of using a program like NIST XCOM is the incorporation of "photon energies immediately above and below all the absorption edges" where discontinuities of the cross sections and total attenuation occur. The program not only separates the coefficients by

individual interaction types but also provides guidance that “the sum of the interaction coefficients for the individual processes is equal to the total attenuation coefficient” (NIST XCOM).

2.5 Elemental Composition of Tissues

One of the dependencies for the absorption and scattering of radiation in a material, is the effective atomic number (Z_{eff}). Due to this Z_{eff}, the research on elemental composition of the human body and its tissues is of vital importance, and has been researched extensively, with the early works of Hawk in 1947 and the creation and refinement of the standard reference man developed from ICRP 23.

2.5.1 ICRP 23

The International Commission on Radiological Protection Publication 23, ICRP 23, titled "Report of the Task Group on Reference Man", published in 1975 provides compiled data on the anatomical, physiological, and metabolic characteristics of a reference individual, often referred to as "Reference Man."

A version of the reference man, or standard man has been used in models since the 1920s. The standard man, a typical Caucasian, western adult male, twenty to thirty years of age, weighing 70 kg, made up of 25 organs and tissues of specific weight, and comprised of 15 elements, was agreed upon by an international committee of health physicists at the Chalk River conference in 1949 to “facilitate comparison of internal dose estimates”. At first only some of the anatomical and physiological data for the respiratory and gastrointestinal tracts was known, but by 1959 ICRP 2 had “vastly extended” this knowledge for the determination of permissible internal doses (Eckerman et al. 1995). The extended data increased the naturally occurring

elements to 46 in 36 tissues, their composition, specific gravity and weights, as well as biological half-lives and deposition parameters (ICRP 23). This work is expanded and refined in current studies (ICRP 110; ICRP 133).

In 1963 a task group was formed to expand on the standard man, reviewing factors of individual variation and characteristics relating to "intake, metabolism, distribution in the body and retention of the various [radionuclides] of concern" (ICRP 23). The publication of ICRP 23 in 1975 was in result of this task group and the standard man was changed to the Reference Man. The Reference man contains data necessary for the estimation of dose from internal and external exposures. Dose estimations are more precise when assumptions are known and small adjustments to values are made from a well-defined reference (Eckerman et al. 1995).

An important feature of ICRP 23 is the elemental composition of organs and tissues. A critical tissue of our research is soft tissue. Soft tissues are a composite tissue and are treated in similar terms as the whole body, the final compositional value is "calculated as the sum of the values for the various (…) tissues." The elemental composition of a tissue is calculated through the known compositions of body components such as water, fat, protein and carbohydrates in the tissue. Table 4 gives the elemental composition of these body components and Table 5 is compiled information that gives the total elemental content in grams of each tissue calculated from the body components from Table 4 (ICRP 23).

Table 4: Elemental composition of select body components (ICRP 23).

Component	Carbon		Hydrogen		Nitrogen		Oxygen	
	%	Ref.	%	Ref.	%	Ref.	%	Ref.
Water			11				89	
Fat	77	33, p. 87	12	33, p. 87			11	33, p. 87
Protein	52	27, p. 27	7	27, p. 27	16	27, p. 27	23	27, p. 27
Carbohydrate	42	33, p. 47	6	33, p. 47			52	27, p. 47
Bone ash							40	9, p. 385

Table 5: Elemental weights in grams for select body tissues (ICRP 23).

Organ and Tissue	Weight (g)	Specific Gravity (g/ml)	Carbon Quantity (g)	Hydrogen Quantity (g)	Nitrogen Quantity (g)	Oxygen Quantity (g)	Potassium Quantity (g)
Total Body	70000	1.07	16000	7000	1800	43000	145*
Total Soft Tissue	60000	--	14000	6300	1500	38000	120

*The potassium quantity has been changed to 145g to reflect the whole-body counter measurement cited in ICRP 23.

2.6 Irradiated Tissue Determination

ICRU 44, titled Tissue Substitutes in Radiation Dosimetry and Measurement, reports on "physical quantities that should be considered when tissue substitutes are selected" and the "important human body tissues requiring simulation" to be used in phantoms and detectors. The first important criteria are "the composition of a tissue substitute chosen for a phantom is based on the composition of the body tissue to be simulated" (ICRU 44). ANSI 13.35 lists the irradiated tissue in a BOMAB phantom as the average soft tissue. The soft tissue composition has been formulated over the years, with notable early works like ICRP 23 and crucial examinations like ICRU 33.

ICRU 33, titled Radiation Quantities and Units, created a phantom model, the ICRU sphere, when analyzing absorbed dose. A 30-cm diameter sphere made up of soft tissue equivalent material of elemental composition: 10.1% H, 11.1% C, 2.6% N 76.2% O representing soft tissue. "Soft tissues may be defined as the body tissues in a human subject other than osseous tissue, teeth, hair, and nails. Soft tissues include all the body fluids, muscle-like tissues, and fatty tissues (e.g., adipose tissue [brain, breast (including component tissues), heart, liver and muscle (skeletal)])" (ICRU 46).

Soft tissue is the most important tissue type to be simulated as it makes up roughly 70% of the body mass of humans (ICRU 44). Soft tissue is not homogeneous and varies from person to person. "Factors such as sex, metabolism, dietary habits, state of health, even elevation above sea level, all play a part in (…) tissue composition (ICRP 23). Consistently, disease, diet, physical activity, age, undernutrition, and overnutrition will all create variation in elemental composition of tissues (ICRU 46). The "differences between people make precise definition of tissue composition nearly impossible" (Griffith 1980).

These variations have led to the development of a standard elemental composition representing the average soft tissue. Average soft tissue compositions have been quoted extensively in ICRP 23, (White 1987), and ICRU publications [ICRU Reports 26 (ICRU, 1977), 33 (ICRU, 1980), 37 (ICRU, 1984b), 44 (ICRU, 1989) and 45 (ICRU, 1990)]" (ICRU 46). The standard ANSI 13.35 uses the average soft tissue defined in ICRU 46 which was quoted from ICRU 44 and developed by White in 1987. The elemental composition of the average soft tissue can be seen below in Table 6.

Table 6: The elemental composition of the average soft tissue (ICRU 46).

Tissue	Hydrogen Composition (Percentage by mass)	Carbon Composition (Percentage by mass)	Nitrogen Composition (Percentage by mass)	Oxygen Composition (Percentage by mass)
ICRU 44 Male Adult Avg. Soft Tiss.	10.5	25.6	2.7	60.2

2.7. Selecting a Tissue Substitute Material

The selection of the material to be used as a tissue substitute material has criteria and guidance listed by ICRU 44. A criterion in the selection of a tissue substitute material is the

comparison of radiation interaction coefficients to within a tolerance of +/-5%. The material itself should be physically sound and chemically compatible, as well as keeping elements with Z>8 less than 1% by weight. Table 7 seen below, gives more non-radiation related criteria.

Table 7: Non radiation related criteria for the selection of a tissue substitute material (ICRU 44).

Type of material	Characteristic	Requirements
All materials	Phase/form	Tissue substitutes are needed as solids, powders, liquids, gels, and gases (White and Constantinou, 1982).
	Composition/purity	The elemental composition must be known within the accuracy dictated by the application. Contaminants must be avoided, especially those of high atomic number ($Z > 20$).
	Homogeneity	Inhomogeneities due to poor dispersion of components or unintentional porosity must not introduce uncertainties in excess of 1% in radiation transmission or dose estimations.
	Stability	Base materials and fillers should be inert. Materials should not degrade under repeated irradiation.
	Toxicity	Noncarcinogenic; hypo-allergenic (IARC, 1972–1984).
Solids	Form	Tissue substitutes may be required as rigid or flexible solids. Materials should be capable of being cast or molded into the required shapes (White *et al.*, 1977; Constantinou, 1978; Griffith, 1980).
	Homogeneity	Small quantities (<1%, by mass) of particulate fillers must be avoided; coarse fillers with mean diameters >100 μm and those that form aggregates (clumping) should be avoided. Inhomogeneities should not be introduced by water absorption or loss.
	Mechanical properties	Rigid solids are required with sufficient mechanical strength to withstand routine handling and they should be capable of being readily machined (milled, turned, drilled, etc.). [The hardness resulting from high loadings (>50%, by mass) of certain particulate fillers (e.g., $CaCO_3$) makes machining difficult.] Minimal warping/creep.
	Thermal properties	Minimal distortion and shrinkage (<0.1%, by volume) by use of low-exotherm, cold-cure resin systems and effective methods of heat removal. (See Appendix C.2.)
	Stability	Plastics containing volatile plasticizers should be avoided.
	Electrical conductivity	In electron beam dosimetry, electrical conductivity may be necessary to avoid charge storage.

2.7.1. Effective Atomic Number Method

During the development of a tissue substitute material, "the use of materials closely simulating the important body tissues is essential if meaningful results are to be obtained" (ICRU 44). ICRU 44 lists three techniques giving guidance on how to formulate tissue substitute material.

The first technique, the Effective Atomic Number (Z) Method, uses a "single effective

atomic number to characterize mass attenuation coefficients over extended energy intervals and is often unsatisfactory". By weighting different atomic numbers of a compound, a coefficient can be derived. Equation (6) and (7) seen below, shows this relationship (ICRU 44).

$$\tau/\rho = a\bar{Z}^x, \qquad \text{Eq. (6)}$$

Where:

a = fraction of electrons contributed by the element

x = number related to an empirical function based on photon energy

$$\bar{Z} = \left(\sum_i \omega_i Z_i^x \right)^{1/x} \qquad \text{Eq. (7)}$$

Where:

W_i = the mass fraction of the ith element with atomic number, Z_i

x = number related to an empirical function based on photon energy

The value of x is a number related to an empirical function based on photon energy. Empirical functions are discussed more in length in Section 3.2.6. The value of 2.94 showed a linear relationship for a small base of compounds at low monoenergetic x-rays (Spiers 1946). This method is found to be insufficient in modern applications with complex compounds and a wide energy range (ICRU 44).

2.7.2. Elemental Equivalence

The second technique, Elemental Equivalence, is the creation of a substitute material simply by replicating the chemical composition of the irradiated tissue as closely as possible. This method has been shown to be useful for even complex scattering and absorption. This "method was used by Rossi and Failla (1956) to formulate a water-based mixture elementally equivalent to an approximate formula for soft tissue, $(C_5H_{40}O_{l8}N)_n$" (ICRU 44).

These four base elements made it possible for early tissue substitute cubic phantoms to be built with materials as simple as water or wax, but in the 1930s, it was found that these simple substitutes were deficient at lower energies, so higher Z_{eff} materials were added to correct these faults (ICRU 48). When developing a mixture, the main ingredient should "approximates tissue with respect to one or more radiation interactions. Other substances are often added to rectify, as far as possible, the deficiencies of the base material" (ICRU 44).

2.7.3. Basic Data Method

The final technique listed is the Basic Data Method. This method is the use of corrective compounds to modify radiation coefficients. This method calculates the fractional weight of the corrective compound, by evaluation of coefficients. Equation (8), seen below, shows this relationship (ICRU 44).

$$\omega_A = \frac{(\tau/\rho)_X - (\tau/\rho)_B}{(\tau/\rho)_A - (\tau/\rho)_B}; \qquad \omega_A + \omega_B = 1,$$

Eq. (8)

Where:

W_A = fractions by mass of A

W_B = fractions by mass of B and

$(\tau / \rho)_X$ = photoelectric mass attenuation coefficient of the tissue

$(\tau / \rho)_A$ = photoelectric mass attenuation coefficient of compound A

$(\tau / \rho)_B$ = photoelectric mass attenuation coefficient of compound B

2.7.4 Polyurethane Urethane

ICRU 44 also gives guidance on the fabrication of tissue substitute material and lists 62 different types of tissue substitute material and their associated references. It is Griffith's research into polyurethane that has shown considerable promise and is outlined in ICRU 44. Polyurethane has a broad range of advantages: flexible or rigid form, commercially available, does not require unique laboratory equipment and can be cast into a wide variety of geometries. Griffiths polyurethane formulations were used to create different tissue types, muscle, adipose, cartilage, bone, and lung (Griffith 1980).

Polyurethane is a polymetric foam that was first synthesized in 1937 by Otto Bayer. At the time, this polymer was considered useless, but has since become a multibillion-dollar industry whose products are practically everywhere, from medicine to space travel. Polyurethane is formed by the reaction of a hydroxyl group (OH) of a polyol with the NCO

group of an isocyanate, forming long polymer chains (Gama 2018). This reaction is seen below in Figure 2.6.

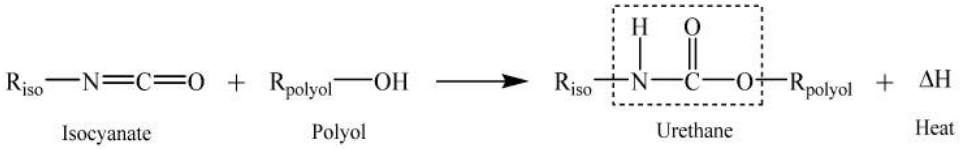

Figure 2.6: The chemical reaction of polyurethane (Gama 2018).

Polyurethane is highly adaptable and can be modified to mimic different tissue types. This modification can be made by changing the amount or types of additives, or by changing the ratio of polyol to isocyanate. Decreasing the polyol ratio will decrease the hardness of the material, while increasing will elongate. Likewise, the different nature of isocyanates will affect the strength and can make the material "rubbery" or more rigid (Gama 2018).

2.8 Other Phantoms

After the introduction of the BOMAB, Alderson developed another anthropomorphic phantom used in dosimetry. The RANDO phantom was designed to mimic the average adult male in terms of size, shape, and tissue composition. It was constructed using tissue-substitute materials, such as plastics and resins, which had radiological properties like human tissues. This phantom allowed researchers and clinicians to assess the distribution of radiation dose in the human body, checking treatment procedures, and evaluate the effects of different radiation therapy techniques (Alderson 1962).

Once computing began to evolve, computational phantoms "which mathematically described the geometries of the bodies and its organ" arose (ICRP 110). The MIRD model was the first generation of such models (Fisher 1967). The second generation of these computational phantoms are called voxel phantoms and are currently defined as the reference phantoms for the

human body (ICRP 110). As stated previously, these phantoms require calibration phantoms and tissue substitute materials for comparison and the determination of certain physical quantities.

2.9 ANSI 13.30

The American National Standard gives guidance for the performance criteria of Radiobioassay. "Radiobioassay measurements are made for the purpose of determining the internal human burden of radioactive material, estimating doses and dose commitments for risk estimates, radiation protection management, medical management where appropriate, and providing the necessary data for legal and record-keeping requirements." The analysis criteria for the performance testing Radiobioassay include bias, precision, and root mean squared error. As well as quality control determinations of the MDA or MDC (ANSI 13.30).

"The testing laboratory shall instruct the service laboratory to determine the amount of radionuclide in a phantom in a minimum of five independent replicate counts for each category in which they are tested. The phantom shall be used to test the service laboratory's relative bias and precision". "Because the actual activity in the person is rarely known for a direct radiobioassay measurement, this criterion applies to measurements on suitable mock-ups, or phantoms, that simulate the person". (ANSI 13.30).

2.9.1 Relative Bias

The relative bias is the deviation of our measurement found by comparing the analytically derived activity against its known activity. The mean relative bias, thought of as the estimate for the average systematic error, is the persistent deviation of our derived value from the true value and is seen below in Equation (9) (ANSI 13.30):

$$B_r = \sum_{i=1}^{N} \frac{B_{ri}}{N}$$

Eq. (9)

Where:

N = number of measurements

B_{ri} = relative bias statistic and is seen below in Equation (10) (ANSI 13.30):

$$B_{ri} = (A_i - A_{ai})/A_{ai}$$

Eq. (10)

Where:

A_i = ith determined value

A_{ai} = known value associated with the ith measurement

2.9.2. Relative Precision

The relative precision, S_B, thought of as the standard deviation or measure of random error, is the degree of agreement of repeated measurements around the mean value. The standard defines it as the "relative dispersion of the values of the [relative bias statistic] from their [mean relative bias]" and can be seen below in Equation (11) (ANSI 13.30):

$$S_B = \sqrt{\frac{\sum_{i=1}^{N} (B_{ri} - B_r)^2}{(N-1)}}$$

Eq. (11)

2.9.3 Root Mean Square Error

The Root Mean Squared Error, seen below in Equation (12) is "a measure of total error defined as the square root of the sum of the square of the relative precision and the square of the relative bias." The root mean square error measures the true dispersion of the measurement as it accounts for both the systematic error and random error, validating the measurement if its value is below 0.25 (ANSI 13.30).

$$RMSE = \sqrt{B_r^2 + S_B^2} \leq 0.25$$

Eq. (12)

The 0.25 value arises from the pragmatic interpretation from the working group of the ANSI 13.30 standard. The standard states any "response should not vary by more than 5% from the established mean", this translates to an upper limit for the absolute value of the random error, denoted as the relative precision, of 5% with an allowable absolute value of the systematic error, denoted as the mean relative bias, of up to roughly 25% (ANSI 13.30).

3. METHODOLOGY

3.1 In-Vivo Counting Systems Hardware

In-Vivo counting systems consist of a detector, cooling system, and multi-channel analyzer with power supply. A fast scan sodium iodine detector is typically used for qualitative purposes for the identification of activity above background, while high purity germanium detectors are used for quantification. The detection system used in this investigation was comprised of a 100% and a 30% relative efficiency, p-type coaxial, PopTop, aluminum capped, high purity germanium detectors. The detector labeled V01 is a large diameter, high efficiency detector, cooled with an ICS-P4 cooling system. The detector labeled DET10 is a small diameter, low efficiency detector, cooled with an X-cooler III. Both detectors use Canberra's Genie 2000 software and Lynx MCA.

Typically, quantitative In-Vivo counting systems are comprised with only large diameter, high efficiency, high purity germanium detectors. It is thought that the inclusion and successful verification of the solid BOMAB on a small diameter, low efficiency, high purity germanium detector reinforces the value of the phantom.

3.2 Genie 2000 Spectroscopy Software

Genie 2000 Spectroscopy Software has "a comprehensive set of capabilities for acquiring and analyzing spectra from multichannel analyzers". The genie software allows for template analysis sequencing for batch routine operations for less experienced technicians, as well as hands on optimization for expert comprehensive analysis (Genie 2017). Due to its wide range of functionality based on individual users, an in-depth look into how and why parameters are defined in the algorithm would be cumbersome and not useful for technicians running routine

work based on their individual procedures. Instead, how the algorithm calculates reported values is shown below.

3.2.1 Activity

The activity the Genie software calculates can be seen below in Equation (13) (Genie 2017):

$$A = \frac{P}{qk\varepsilon bE_1} \; x \; e^{\lambda Ts} \; x \; \frac{\lambda E_r}{(1 - e^{-\lambda E_r})}$$

Where:

A = calculated specific activity (µCi/unit)
P = corrected peak area (i.e., net counts)
q = sample quantity (e.g., grams)
k = 37000 disintegrations/second/µCi (i.e., Becquerels /µCi)
ε = the calculated efficiency (in counts/gamma)
b = the branching ratio (in gammas/disintegration)
E_l = elapsed live time (in seconds)
e = the constant e equals 2.7182818..., the base of the natural logarithm
λ = the radionuclide decay constant (i.e., ln (2) / half-life of the radionuclide in seconds)
T_S = decay time in seconds from sample collection time to acquisition start time (acquisition start time – sample collection time in seconds)
E_r = elapsed real time (in seconds)

Eq. (13)

3.2.2 Activity Uncertainty

The uncertainty of the activity the Genie software calculates can be seen below in Equation (14) (Genie 2017):

$$\Delta A = A \; x \; \sqrt{\left(\frac{\Delta P}{P}\right)^2 + \left(\frac{\Delta b}{b}\right)^2 + \left(\frac{\Delta \varepsilon}{\varepsilon}\right)^2 + \left(\frac{SYS}{100}\right)^2 + \left(\Delta\, Decay\right)^2}$$

Where:

$$\Delta\, Decay = \left(\frac{\Delta T_{1/2}}{T_{1/2}}\right) x \left(\frac{\lambda E_r}{1 - e^{-\lambda E_r}} - \lambda(T_s + E_r) - 1\right)$$

ΔA = the uncertainty in the calculated specific activity A

ΔP = the uncertainty in the corrected peak area P

Δb = the uncertainty in the branching ratio (gammas/disintegration)

$\Delta \varepsilon$ = the uncertainty in the efficiency ε (this incorporates the total uncertainty of the calibration standard and other uncertainties in the efficiency measurement)

SYS = the systematic error estimate in percent; this is a user-definable estimate to incorporate uncertainties in sample quantity, sample positioning, counting geometry, sample matrix effect, and other sample or counting uncertainties (estimated at one standard deviation)

$\Delta T_{1/2}$ = the uncertainty in the radionuclide half-life

Eq. (14)

3.2.3 Efficiency Development

There are several methods for the generation of a calibration curve, by certificate file, calibration file, manual entry, or nuclide list. The chosen method for this investigation was a combination of nuclide list and manual entry. Nuclide list allows the entry of the assay date and time, the Activity, uncertainty and preferred units for each individual nuclide. Manual entry allows the manipulation of energy parameters expressed in units of keV so that can be made to match chosen reference values and the further modification of efficiency values (Genie 2017).

3.2.4 Efficiency Calculation

After the entry of parameters into the nuclide list, the genie software will auto populate the efficiency and its associated uncertainty for each calibration point. The efficiency the Genie software calculates can be seen below in Equation (15) (Genie 2017):

$$\varepsilon = \frac{P}{QRE_1} \; x \; e^{\lambda Ts} \; x \; \frac{\lambda E_r}{\left(1 - e^{-\lambda E_r}\right)}$$

Where:

ε = the calculated photopeak efficiency (in counts/gamma)

P = the corrected peak area (i.e., net counts)

Q = the calibration source quantity in units used (e.g., grams, mL, etc.)

R = the efficiency calibration source emission rate in gammas/second/unit

E_l = the elapsed live time (in seconds)

e = the constant e equals 2.7182818..., the base of the natural logarithm

λ = the radionuclide decay constant (i.e., ln (2) / half-life of the radionuclide in seconds)

T_S = the decay time in seconds from sample collection time to acquisition start time (acquisition start time – sample collection time in seconds)

E_r = the elapsed real time (in seconds)

Eq. (15)

3.2.5 Efficiency Uncertainty

The uncertainty in the efficiency the Genie software calculates can be seen below in Equation (16) (Genie 2017):

$$\Delta\varepsilon = \varepsilon \; x \sqrt{\left(\frac{\Delta P}{P}\right)^2 + \left(\frac{\Delta R}{R}\right)^2 + \left(\frac{\Delta T_{1/2}}{T}\right)^2 x \left(\frac{\lambda E_r}{1 - e^{-\lambda E_r}} - \lambda(T_S + E_r) - 1\right)^2}$$

Where:

$\Delta\varepsilon$ = the uncertainty in the calculated efficiency ε at the calibration point

ΔP = the uncertainty in the corrected peak area P obtained from the peak search results

ΔR = the uncertainty in the gamma-ray emission rate obtained from the calibration standard certificate and entered into the certificate file

$\Delta T_{1/2}$ = the uncertainty in the radionuclide half-life obtained from radioactive decay references and entered into the certificate file

Eq. (16)

The typical uncertainty in the efficiency for points calibrated directly is roughly 2-5%. This is dependent on the errors propagated from the original standard certificate, or nuclear data sheets. The uncertainty can also be inflated by diminished resolution of the detection system, low counting times, or improper energy calibration. Additional uncertainty is generated for extrapolated points on the efficiency curve, discussed further in Sections 3.2.8 and 3.2.10.

3.2.6 Empirical Efficiency Curve

Equation (15) and Equation (16) are equations to determine the efficiency at calibrations points of specific energy. An efficiency curve uses a system of interpolation to determine efficiencies of points that lie outside these specific energies. The two types of interpolated efficiencies used in this investigation are an empirical fit and a cubic spline fit. The empirical fit uses a weighted least square fit polynomial that may or may not pass through each calibration point but uses a "best fit" efficiency curve. The empirical fit efficiency points are calculated below in Equation (17) (Genie 2017):

$$1n(\varepsilon) = a_2 + a_3 + a_4(x)^2 + a_5(x)^3 + a_6(x)^4 + a_7(x)^5$$

Where:

ε = the calculated efficiency in counts/gamma
$x = \ln(a_1/E)$
E = peak energy (in keV) at which the efficiency is calculated
$a_1 = (E_1 + E_2) / 2$
E_1 = the smallest calibration energy
E_2 = the largest calibration energy
a_2 through a_7 = the fit parameters

Eq. (17)

The empirical curve developed from the solid BOMAB, and the analysis of its approximation is found in Section 4.2.

3.2.7 Empirical Fit Parameters

The order of the polynomial n, seen in Equation (17), is dependent on the number of calibration points. The value of n is seen below in Table 8.

Table 8: The polynomial order to Equation (17), per number of calibration points (Genie 2017).

n value	Calibration Points
5	10+
4	8-9
3	6-7
2	3-5

The number of fit parameters seen is Equation (17), is n+2. The value of the fit parameters a, is seen below in Equation (18) (Genie 2017):

$$\overline{M} * a = \overline{V}$$

Where:

$$M_{jk} = \Sigma_i W_i * [\ln(a_1/E_i)]^{j-1} * [\ln(a_1/E_i)]^{k-1}$$

$$V_k = \Sigma_i W_i * \ln(\varepsilon_i) * [\ln(a_1/E_i)]^{k-1}$$

Where:

$$W_i = (\varepsilon/\sigma_\varepsilon)^2$$

Where:

$$\sigma_\varepsilon = \Delta\varepsilon_{E_1} + [(\Delta\varepsilon_{E_2} - \Delta\varepsilon_{E_1})/(E_2 - E_1)] * (F-E_1)$$

Where:

$\Delta\varepsilon_{E_1}$ = uncertainty at E_1

$\Delta\varepsilon_{E_2}$ = uncertainty at E_2

F = Efficiency computed by curve

Eq. (18)

3.2.8 Empirical Uncertainty

The fit parameters are solved in the above equation by inverting the M matrix. A typical matrix equation would establish covariance terms for error propagation, instead the empirical uncertainty is a root mean squared sum, seen below in Equation (19) (Genie 2017):

$$\Delta\Phi = \left[\Delta\varepsilon^2 + \left(F - \varepsilon\right)^2\right]^{1/2}$$

Where:

$\Delta\Phi$	=	the interpolation uncertainty
$\Delta\varepsilon$	=	the calculated uncertainty in the efficiency
ε	=	the calculated efficiency
F	=	the efficiency predicted by the empirical equation

Eq. (19)

3.2.9 Cubic Spline Fit Efficiency

The cubic spline fit is a third order piecewise polynomial that is continuous and smooth through its boundaries. This efficiency curve will pass through each calibration point but cannot extrapolate past its lowest and largest calibration point energies. Similarly, any use of efficiency data from an extrapolated area should be used with caution as the curve may not be a best fit, especially with minimal or widespread points. The extrapolated cubic spline efficiency is calculated below in Equation (20) (Genie 2017):

$$\ln(\varepsilon) = \ln(\varepsilon_n) + \{[\ln(\varepsilon_{n+1}) - \ln(\varepsilon_n)]/[(\ln(E_{n+1}) - \ln(E_n)]\} * [\ln(E) - \ln(E_n)]$$

$$\text{For: } E_n < E < E_{n+1}$$

Eq. (20)

The cubic spline curve developed from the solid BOMAB is found in Section 4.2.

3.2.10 Cubic Spline Uncertainty

The uncertainty of the efficiency for the extrapolated points is calculated below in Equation (21) (Genie 2017).

$$\ln(\Delta\varepsilon) = \ln(\varepsilon_n+\Delta\varepsilon_n)+\{[\ln(\varepsilon_{n+1}+\Delta\varepsilon_{n+1})-\ln(\varepsilon_n+\Delta\varepsilon_n)]/[\ln(E_{n+1})-\ln(E_n)]\}*[\ln(E)-\ln(E_n)] \quad \text{Eq. (21)}$$

3.2.11 Energy Calibration

There are several methods for the completion of a standard energy calibration, by certificate file, calibration file, manual entry, coefficient values or nuclide list. Typically, a detector is energy calibrated during its initial set up and is periodically updated with its background, but inspection and recalibration may be required. The chosen method of energy calibration for this investigation is entry by nuclide list.

Energy calibration includes the examination of FWHM, low-tail and verification of energy/channel pairs. Nuclide list allows the manual identification of the peak ROIs so the energy calibration can be altered based on the technician's experience (Genie 2017). The energy calibration developed from solid BOMAB and the fit of the data is shown in Section 4.2.

3.3 BOMAB Criteria

3.3.1 Dimension Criteria

Section 3.3.1 through 3.3.3 details the verification of the shells as ANSI 13.35 compliant. ANSI 13.35 gives criteria on the fabrication of the BOMAB. The first criteria are the match of the physical dimensions. Table 9 and 10 compare the measured values against the criteria tolerances and are shown to be within acceptable tolerances.

Table 9: The criteria for cross-sectional dimensions and their associated tolerances compared against measured values.

Section	Dimension 2a (cm) +/- 5%	Measure 2a (cm)	Measured/ criteria	Dimension 2b (cm) +/- 5%	Measured 2b (cm)	Measured/ criteria
Head	14	14	1.000	19	19	1.000
Neck	13	12.4	0.954	13	12.4	0.954
Thorax	20	19.5	0.975	30	28.6	0.953
Abdomen	20	20	1.000	36	34.9	0.969
Thighs	15	14.5	0.967	15	14.5	0.967
Calves	12	12	1.000	12	12	1.000
Arms	10	9.8	0.980	10	9.8	0.980

Table 10: The ANSI 13.35 criteria for cross-sectional dimensions and their associated tolerances compared against measured values.

Section	Height (cm) +/- 5%	Measured Height (cm)	Measured/ criteria	Thickness (cm) +/- 10%	Measured Thickness (cm)	Measured/ criteria
Head	20	19.6	0.980	0.5	0.5	1.000
Neck	10	9.9	0.990	0.5	0.5	1.000
Thorax	40	38.5	0.963	0.5	0.5	1.000
Abdomen	20	19.8	0.990	0.5	0.5	1.000
Thighs	40	38.5	0.963	0.5	0.5	1.000
Calves	40	38.5	0.963	0.5	0.5	1.000
Arms	60	58	0.967	0.5	0.5	1.000
Total	170*	164.8*	0.969			

*: Total Height does not include arm measurements.

3.3.2 Volume Criteria

After confirmation of these criteria the shells were counted in the In-Vivo counting system to identify any radioactive contamination. An overnight count did not display any activity above background. The shells were then washed with a 5% nitric solution, rinsed with deionized water, and dried. Once dried, the bottles were weighed empty, and then weighed again filled with de-ionized water. This establishes fill volumes are consistent with the criteria of our ANIS 13.35 standard and to calculate any allowable expansion of the fill material.

Table 11: The ANSI 13.35 criteria for fill volume and their associated tolerances compared against measured values.

Section	Fill Volume (cc) +/- 16%	Measured Fill Volume (cc)	Measured/ criteria
Head	3490	3366.20	0.965
Neck	1020	960.00	0.941
Thorax	1690	15355.10	0.909
Abdomen	9920	8733.40	0.880
Thighs	6000	11779.40	0.982
Calves	3710	8209.30	1.106
Arms	3750	8074.50	1.077
Total	58200**	56477.90	0.970

**: Total Fill Volume includes twice the value of arms, thighs, and calves.

3.3.3 Shell Criteria

The next criterion is the attenuation coefficients of the shell. The chemical composition of the shell is polyethylene, with a density listed on the SDS at roughly 938 (kg/m^3), which is within 2% of criteria, and within acceptable tolerance. Table 12, seen below compares the mass attenuation coefficients of the shells and the average soft tissue of ICRU 46. The comparison of these values is within acceptable tolerances.

Table 12: Mass attenuation coefficients for ICRU 46 Average soft tissue as listed in ANSI 13.35 vs NIST XCOM calculated shell mass attenuation coefficients

Photon Energy (MeV)	Criteria Mass Attenuation Coefficient (m^2/kg)	NIST XCOM Shell Mass Attenuation Coefficient (m^2/kg)	Ratio Acceptance +/- 10%
0.1	0.01690	0.01720	1.018
0.2	0.01360	0.01400	1.029
0.5	0.00960	0.00995	1.036
1.0	0.00700	0.00726	1.037
1.5	0.00570	0.00591	1.037
2.0	0.00490	0.00506	1.033
2.5	0.00430	0.00448	1.042
3.0	0.00393	0.00405	1.031

ANSI 13.35 does not provide a quantitative checklist on the criteria of sturdiness, but ANSI 13.35 suggests a qualitative inspection to be made to ensure the shells are free from cracks or defects. A leak test was also administered over a 24-hour period and no leaks were found. No quantitative checklist is provided for the chemical compatibility between the filler material and shell, but ANSI 13.35 lists polyethylene as a material that meets the criteria of chemical compatibility.

3.4 Tissue Substitute Material Criteria

The next stage of this investigation is the selection of a tissue substitute material. ICRU 44 has a large list of different tissue substitutes of which urethane is listed as a suitable material. ICRU 44 has a list of criteria that was considered during the determination of a tissue substitute material.

3.4.1 Elemental Equivalence

First, urethane satisfies the technique of selection, Elemental Equivalence. "The typical composition of polyurethane is 8-10% H, 60-65% C, 3-4% N, and 20-25% 0, by mass. Except for reversal of the carbon oxygen concentrations, the nominal composition of polyurethane is not severely different from that of soft body tissues". Selection of a material with a similar elemental composition will satisfy the criteria of approximating one of more radiation interactions by matching the probability of interaction through the effective atomic number (ICRU 44).

3.4.2 Non radiological criteria

As previously stated, urethane has a list of advantages that are compatible to the criteria listed in Table 7. The base element composition is inert and has no atomic numbers larger than 8, is non-carcinogenic and is only a mild irritant and skin sensitizer in its non-solid form. As a solid it is considered a non-hazardous waste, that can be made rigid or flexible, cast into a variety of geometries, and stable with a high tensile and flex strength (ICRU 44).

3.4.3 Main Component Selection

There are many commercially available urethanes to choose from. A list of potential urethanes was made, considering availability, lead times for shipping and the availability of an SDS directly from the vendor. The SDS gives the chemical formula for elemental composition comparison, as well as specific gravity. These are necessary data used as inputs to determine attenuation coefficients through NIST XCOM.

ScotchCast, Adeprene, Tc-284 and Alumilite were the main components considered. One-liter small proof of concepts was built to test expansion properties and the curing process of each material. It was found that ScotchCast cured too slowly, which could create homogeneity problems as non-soluble potassium salts precipitate. A blank bolus phantom created for tissue back scatter experiment took weeks to fully cure in its mold, experience therefore dictated that ScotchCast cured too slowly. Tc-284, which is a polyurethan foam, had a large expansion coefficient making the density value fall outside of criteria tolerances. Adeprene had a three-month lead time and fell outside critical deadlines. Alumilite was chosen as the main ingredient for this investigation as it cured quickly, matched criteria, and was readily available even from local distributors. Table 13, seen below shows the density criteria comparison of our mixture with the ANSI 13.35 standard.

Table 13: The density criteria comparison of our mixture with the ANSI 13.35 standard.

Section	Density Criteria (kg/m^3)	Density SDS (kg/m^3)	SDS / Criteria
Filler	1005 +/- 5%	1040	1.035

3.4.4 Additive

The technique of elemental equivalence has historically demonstrated excessive differences in low energy attenuation coefficients as compared to tissue. So, it is well known that when using this technique, a corrective compound is necessary (ICRU 44). Griffiths research has shown calcium carbonate at 4.3% by weight is an adequate filler for a wide range of applications (Griffith 1980). Manipulation of this percentage allows adequate simulation of a large variety of tissue types (ICRU 44). Using different concentrations of Calcium carbonate in

conjunction with polyol ratio manipulations allows for the modification of one formulation to fit a wide range of different tissue groups like muscle, breast, adipose, cartilage, bone, and lung (Griffith 1980). It was found that no additive was necessary for the energy range set forth in ANSI 13.35, but calcium carbonate was used to test the validity of its use in future tissue studies, such as the use of transuranic elements in the phantom when low energy x-rays require analysis.

3.4.5 Potassium

Given that the additive and main ingredients to be employed in this investigation had been determined, the potassium salt used for background and MDA had to be established. Potassium Chloride, Potassium carbonate, potassium hydroxide, and potassium acetate were all analyzed, by one-liter small scale experiments. Potassium hydroxide is hygroscopic so a true weight measurement would be difficult as the fractional water weight can be as high as 15%. Additionally, potassium hydroxide is sold in bulk as pellets, flakes or in solution, which would not be beneficial to this investigation as clumping could create inhomogeneity. Potassium Chloride was determined to be a viable source of K-40 but tended to precipitate out of solution during experiments. Potassium acetate was considered due to its use as a catalyst in the production of polyurethanes (Hosea 2005). An increased rate to our chemical reaction was unnecessary, so it was rejected in favor of our final selection.

Potassium carbonate was ultimately chosen due to its double potassium, triple oxygen, and fine powder consistency for homogeneity. The addition of calcium carbonate and potassium carbonate helps to increase the oxygen element of a mixture as “polymers and resins [are] handicapped by the deficient oxygen content of these materials compared to most body tissues (ICRU 44).

3.4.6 ^{40}K Activity

The method to calculate activity of the spiked potassium, is seen below in Equation (22). Values calculated with this expression were verified against a calibration source of a known aqueous solution of potassium hydroxide. This provided insights into solubility and homogeneity. The results of this verification are seen below in Table 14.

$$A(pCi/g) = \frac{Ab_{40K} \cdot M_{K_2} \cdot N_A \cdot P_{K_2CO_3} \cdot \lambda_{40K}}{M_{K_2CO_3} \cdot X_{40K} \cdot (0.037)} \quad \text{Eq. (22)}$$

Where:

Ab_{40K} = fractional abundance of ^{40}K in natural potassium

M_{K2} = molar weight of two potassium

N_A = Avogadro's number

P_{K2CO3} = the fractional purity of the salt

λ = decay constant

M_{K2CO3} = molar weight of potassium carbonate

X_{40K} = atomic weight of ^{40}K

0.037 = conversion from Becquerels to picocuries

The activity concentration of our potassium salt, K_2CO_3, was found to be approximately 459 pCi/g.

3.4.7 ^{40}K Verification

The verification of the ^{40}K value was performed on three separate high purity germanium detectors.

Table 14: Verification results of our potassium salt.

Nuclide and Energy (keV)	Counted Activity (pCi/g)	Rounded Average Activity (pCi/g)	Relative % standard deviation	Calculated Activity (pCi/g)	Relative Bias %
^{40}K @1460.8	451.5 465.6 481.5	466	3.2	459	1.5

3.5 Spiking Method

Development of a spiking method was necessary for this investigation. It was known apriori that the traditional way of spiking; the addition of an aliquot of a nitric solution directly into the material, was problematic as the addition of any water into the proposed mixture added unwanted frothing and expansion with the production of carbon dioxide (Gama 2018). Griffith's method of spiking was "dissolving the radionuclide in nitrate form, together with a small amount of lanthanum nitrate carrier, in acetone" was therefore alternately employed (Griffith 1980). The acetone solution is soluble in the proposed mixture and has a high evaporation rate making this subjectively a viable method for reproducibility. The spiking method used in this investigation was developed by RESL. RESLs spiking methods are highly effective but are a closely held trade secret.

3.5.1 Verification of Spiking Method and Homogeneity

A small-scale experiment verifying the spiking method and its homogeneity was conducted by spiking the mixture with ^{137}Cs in a one-liter bottle and comparing that to a NIST traceable calibration standard. The verification of the ^{137}Cs value to within 1% was performed on three separate high purity germanium detectors. The results of this verification are seen below in Table 15.

Table 15: Verification of the spiking method and its homogeneity.

Nuclide and Energy (keV)	Counted Activity (pCi/g)	Rounded Average Activity (pCi/g)	Relative % stdev	Calculated Activity (pCi/g)	Relative Bias %
^{137}Cs @661.65	419.4 422.6 428.7	424	1.1	420	0.95

The verification of the cesium and potassium standard in such a precise manner shows that the shaking of the volume is enough to ensure homogeneity, indeed "only vigorous mixing is needed to achieve a homogeneous casting" (Griffith 1980).

3.6 Radionuclide Selection and Activity

Experience dictates that the generation of a calibration curve that satisfies the energy criteria of ANSI 13.35 requires specific radionuclide(s). There should be a few peaks dispersed within the spectra with a peak near 100keV, and a final peak near the tail of the curve as it becomes near asymptotical. The radionuclide(s) should be moderately long lived with activity and branching ratios high enough to last several years and produce enough counts within their peaks that counting time is reasonable. Furthermore, the comparison against a NIST traceable

calibration standard requires radionuclides that match so verification can occur with maximal precision, using interpolated calibration points.

ANSI 13.30 givess insights into a potential activity. The upper bound test ranges are twenty times the minimum testing levels. Table 28, seen in Appendix 1 lists the minimum testing level for total body nuclides at 81 nCi. A calibration phantom is not bound by testing ranges, but the ANSI standard confirms the capabilities of most users at thousands of nanocuries. To facilitate shipment, the activities used in a phantom ideally should not exceed 49 CFR 173.436 exempt limitations.

The nuclide that satisfies the conditions listed above is ^{152}Eu. An appropriate activity was estimated using Equation (23) and (24). An example spike amount and activity of the solution is seen in Table 16 below.

$$\frac{\frac{10000\ cts}{GPS}}{Det\ (eff)} = \text{Time (seconds)} \qquad \text{Eq. (23)}$$

Where:

$$GPS = A * BR * (0.037) \qquad \text{Eq. (24)}$$

Where:

GPS = gammas per second

A = Activity in picocuries,

BR = branching ratio,

Det(eff) = efficiency of the detector at a specified energy

0.037 = conversion factor from picocuries to becquerels.

10,000 counts = required amount to reduce counting uncertainty to 1%.

Table 16: The time required to achieve ten thousand counts in the peak area if 5 ml of the standard is taken.

Nuclide	Gamma Energy (keV)	Half-life (d)	BR (%)	Decay Date	Decay Activity (pCi/g)	Spike (g)	GPS	DET eff	Time (s) required 10k counts
^{40}K	1460.8	4.66E+11	10.67	5/16/23	459	306	554	0.00021	86337
^{152}Eu	121.8	4939	28.41	5/16/23	472406	5	24829	0.00039	1045
^{152}Eu	344.3	4939	26.59	5/16/23	472406	5	23238	0.00035	1227
^{152}Eu	1112.1	4939	13.41	5/16/23	472406	5	11720	0.00024	3518
^{152}Eu	1408	4939	20.85	5/16/23	472406	5	18222	0.00021	2571
^{152}Eu	1457.6	4939	0.49	5/16/23	472406	5	435	0.00021	115461

The example spike amount seen above in Table 16 would give a total activity of 2.36 +/- 0.05 microcuries, which is near the upper bound testing level, and falls below the 27 microcuries value listed in 49 CFR 173.436 "Activity limit for exempt consignment" table seen in Appendix 2. ANSI 13.35 recommends a ^{40}K activity of approximately 120 nCi/tot, but this investigation elected to increase this value to 140 nCi/tot. The additional activity increases the gammas per second in order to more easily resolve of the ^{40}K 1460 keV peak and the ^{152}Eu 1458 keV peak.

3.7 NIST XCOM Attenuation

Using NIST XCOMs mixture tab with known fractional weights a comparison of calculated attenuation coefficient values to the standard's attenuation values was completed. Table 17 seen below, is the chemical formula and fractional weights of the compounds. Some of the compounds have been redacted to protect proprietary information, the remaining fractional weights have been normalized, this normalization did not change the attenuation values in a meaningful way. Table 18 seen below, are the NIST XCOM calculated values compared to our ANSI 13.35 standard.

Table 17: Chemical formula of the compounds in our mix and their fractional weights.

Chemical Formula	Wt%	Description
C14H31NO	23.5	Propoxylated Amine
C16H30O4	23.5	2,2,4-trimethyl-1, 3-pentanediol dissobutyrate
C12H44O4Sn	0.5	Dimethyltin neodecanonate
C15H22N2O2	42.75	4, 4'-methylene di(cyclohexyl isocyanate)
C8H12N2O2	4.75	Hexamthylene diisocyanate oligomers
CaCO3	4.3	Calcium carbonate for tissue equivalent attenuation
K2CO3	0.7	Potassium Carbonate for background ^{40}K

Table 18: NIST XCOM's calculated attenuation for the tissue substitute compared to the coefficients defined in ANSI 13.35.

MeV	keV	Soft Tissue Mass Attenuation Coefficient (m^2/kg)	Tissue Substitute Mass Attenuation Coefficient (m^2/kg)	Acceptance .+/-5%
0.015	15	0.160	0.164	1.025
0.1	100	0.01690	0.01703	1.008
0.2	200	0.01360	0.01352	0.994
0.5	500	0.00960	0.009547	0.994
1	1000	0.00700	0.006967	0.995
1.5	1500	0.00570	0.00567	0.995
2	2000	0.00490	0.004864	0.993
3	3000	0.00393	0.003898	0.992

ANSI 13.35 only requires comparison of the energy range from 100 to 3000 keV, but the additional point of 15 keV was included to validate the justification of the calcium carbonate additive. Table 30, seen in Appendix 3 shows the comparison of attenuation coefficients without the additive, which would fail at low x-ray energies. The 17-keV point is vital in transuranic studies.

3.8 BOMAB Fabrication

The fabrication of the solid BOMAB was done per "limb" in accordance with the Radiological and Environmental Sciences Laboratory BOMAB procedure for re-spiking, which is the fractional percentage per volume of the fill dimensions of ANSI 13.35, seen below in Table 19.

Table 19: BOMABs fractional percentage per volume based on ANSI 13.35.

Section	Fill Volume (cc) +/- 18%	w/v%
Head	3490	6
Neck	1020	1.8
Thorax	16900	29
Abdomen	9920	17
Thighs	6000	10.3
Calves	3710	6.4
Arms	3750	6.4
Total	58200**	100

**: Total Fill Volume includes twice the value of arms, thighs and calves.

The potassium salt, calcium carbonate additive, spike and part A were mixed prior to the addition of the isocyanate mixture, part B. This helped to ensure at least a 50% homogeneity and can be qualitatively checked due to the translucent quality of part A. The final solidified product qualitatively speaks to the final homogeneity as it will only solidify entirely if both parts are mixed completely. The final verification of the solid BOMAB and its use in verifying a performance testing BOMAB is a quantitative check on its homogeneity as in-vivo count systems are geometry sensitive. After the tissue substitute material has cured the BOMAB was further sealed using silicone on the caps.

3.8.1 BOMAB Activity and Uncertainty

The activity of the BOMAB is determined by the concentration activity multiplied by the total amount of spike used. The "uncertainty is taken as the original nuclide certificate uncertainty as the dilution mass uncertainty adds a negligible portion", the standardized certificate, performed by RESL, carries a 2% uncertainty (RESL 2023). The calculated values are seen below in Table 20.

Table 20: BOMAB calculated activity and uncertainty.

Solution	Isotope	Activity Concentration (pCi/g)	Spike Amount (g)	Activity (pCi)	Uncertainty (pCi)	Date
^{152}Eu 78660	^{152}Eu	472000	4.826	2280000	50000	5/16/23

3.9 BOMAB Verification and Calibration

The BOMABs were counted using the system defined in Section 3.1 and 3.2. The BOMABs were counted in 5 separate measurements, long enough for at least 10000 counts to be collected in each peak lowering the counting uncertainty to 1% or less. The results were statistically analyzed using the ANSI 13.30 methods described in Section 2.9. All standard solutions and performance testing phantoms used are NIST traceable and all current and future manufacturing is required to be done by a trained technician in ISO/IEC 17025:2017, ISO 17034 and ISO 17043, whose work has been shown to be NIST traceable.

4. RESULTS

4.1 Solid BOMAB Verification

The Solid BOMAB was verified using a cubic spline interpolated efficiency curve developed from NIST traceable BOMAB containing ^{152}Eu, "PL-Eu-152-1" and cross verified with a separate standard lineage from NIST traceable BOMAB containing ^{152}Eu, "INL-2006". The results of this verification can be seen below in Table 21.

Table 21: Verification results for Solid BOMAB.

Nuclide and Energy (keV)	**^{40}K @ 1460.81**	**^{152}Eu @ 121.78**	**^{152}Eu @ 344.27**	**^{152}Eu @ 1112.02**	**^{152}Eu @ 1407.95**	**^{152}Eu @ 1457.95**
Count 1 Activity	145.3	2277.7	2249.8	2256.8	2263.3	N/A
Count 2 Activity	139.7	2371.1	2379.9	2359.6	2327.4	N/A
Count 3 Activity	143.69	2259.6	2249.1	2215.8	2223.6	2213.5
Rounded Average Activity	143	2300	2290	2280	2270	2200
Relative stdev %	2.0	2.6	3.3	3.3	2.3	N/A
Calculated Activity	140	2280	2280	2280	2280	2280
Relative Bias %	**2.1**	**0.9**	**0.4**	**0.0**	**-0.4**	**-3.5**

*Listed activities are nCi/tot

Typically, ^{40}K would not be used in conjunction with ^{152}Eu in a calibration standard as the 1460 keV and 1458 keV peak respectively, are too close to calibrate for both and require additional work to verify. ^{40}K was added to this calibration standard to show the efficacy of its addition to future phantoms for its intended purpose of background and MDA determinations. Only one verification result is shown for the 1458 peak due to the additional counts time to resolve the peaks, as well as the cubic spline interpolation calibration curve not being calibrated directly at the 1458 point.

4.2 Solid BOMAB calibration

The Solid BOMAB was counted for roughly one hour, till ten thousand counts or more were seen in each peak of interest. The calibration points of interest, excluding 1458, can be seen in Table 21 above. The five-point calibration was used to develop two calibration curves for each detector, an empirical and cubic spline curve. The empirical curve for V01 can be seen below in Figure 4.1 while Figure 4.2 shows the cubic spline curve.

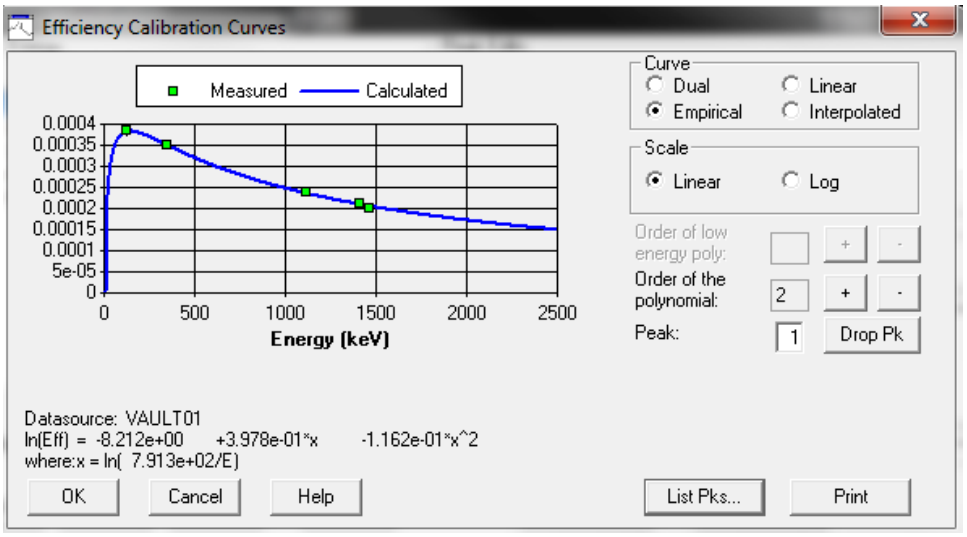

Figure 4.1: V01 empirical curve developed from the solid BOMAB.

As discussed previously, the empirical curve is said to be a "best fit" curve, which passes by each point as close as possible. A good measure of the curve fitting would then be to measure the deviation between the empirical efficiency curve and the points of interest. Table 22 seen below, is the algorithms calculated deviation of the empirical curve for V01 and validates the curve as a good fit for the purpose of this investigation.

Table 22: The deviation of the V01 empirical curve as calculated by Genie.

Peak (keV)	**121.78**	**344.27**	**1112.02**	**1407.95**	**1460.81**
Deviation (%)	-0.18	0.59	-1.24	-1.36	2.24

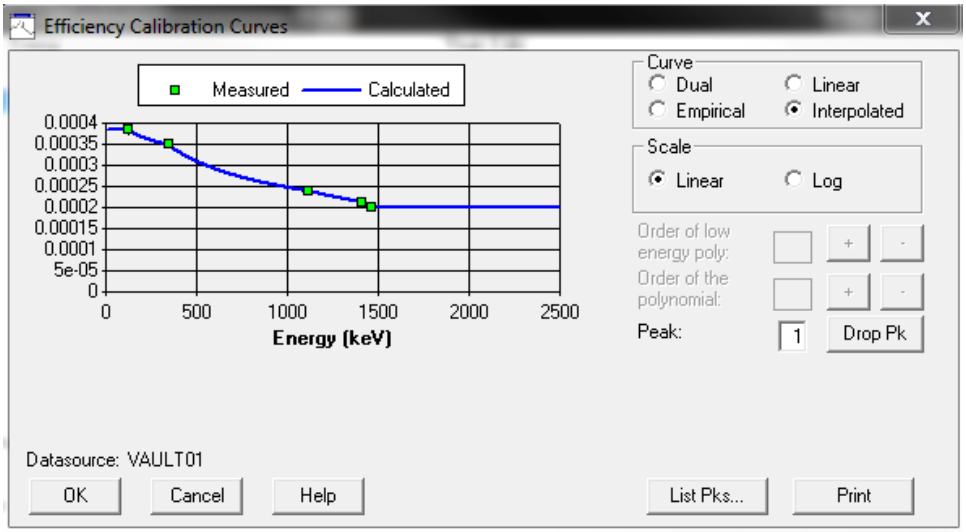

Figure 4.2: V01 cubic spline curve developed from the solid BOMAB.

The fit of the cubic spline curve ought not be tested in a similar method to the empirical curve, as the curve does pass directly through each point. Instead, a better test of the curve is the mean relative bias of the performance testing BOMAB, which can be seen below in Table 25.

The empirical curve for DET10 can be seen below in Figure 4.3 while Figure 4.4 shows the cubic spline curve.

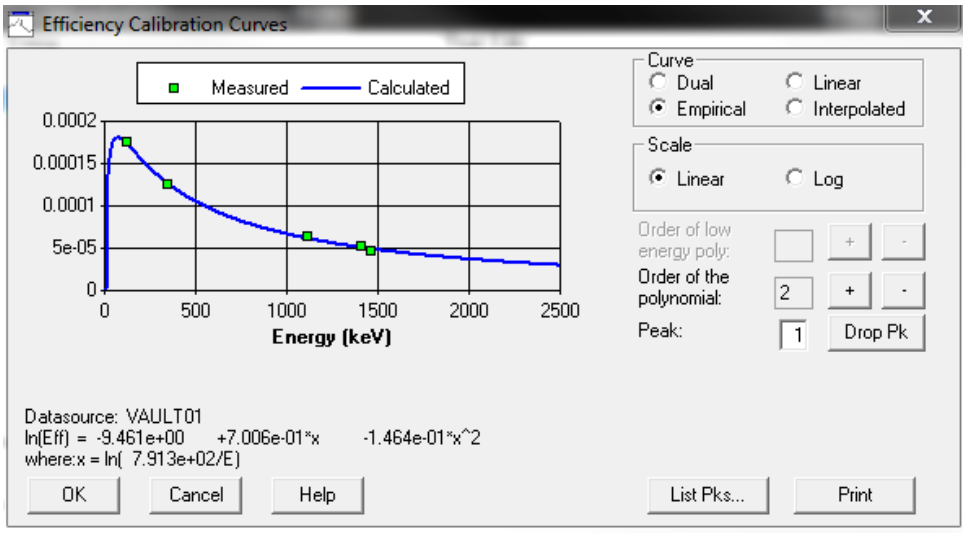

Figure 4.3: DET10 empirical curve developed from the solid BOMAB.

Table 23 seen below, is the algorithms calculated deviation of the empirical curve for DET10 and validates the curve as a good fit for the purposes of this investigation.

Table 23: The deviation of the DET10 empirical curve as calculated by Genie.

Peak (keV)	**121.78**	**344.27**	**1112.02**	**1407.95**	**1460.81**
Deviation (%)	-0.44	1.42	-3.08	-2.5	4.8

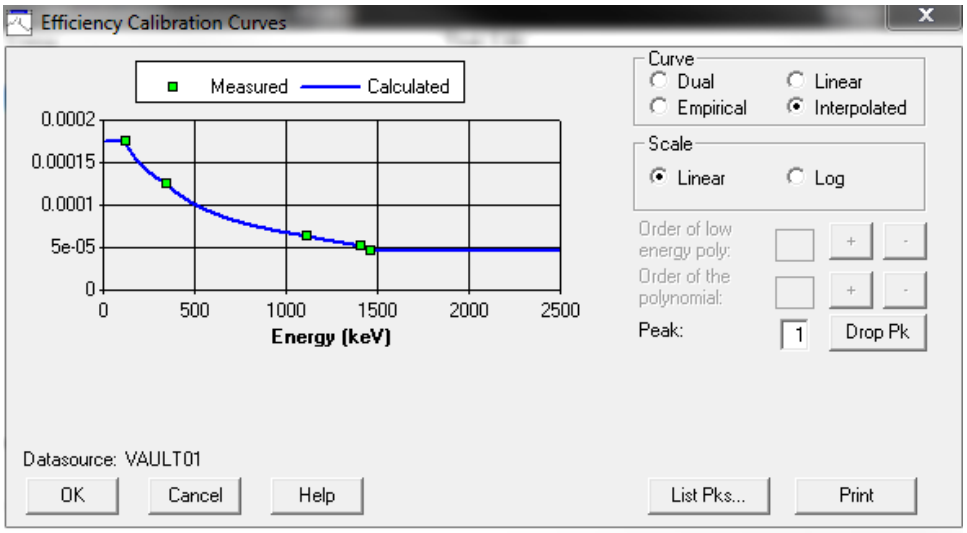

Figure 4.4: DET10 cubic spline curve developed from the solid BOMAB.

The energy calibration for V01 is seen below in Figure 4.5 while DET10 is seen in Figure 4.6. The relationship between channels and energy is linear, every channel representing 0.5 keV. The calibration is thought to be a good fit for both detectors as the slope of the line is 0.5 and the intercept being approximately zero.

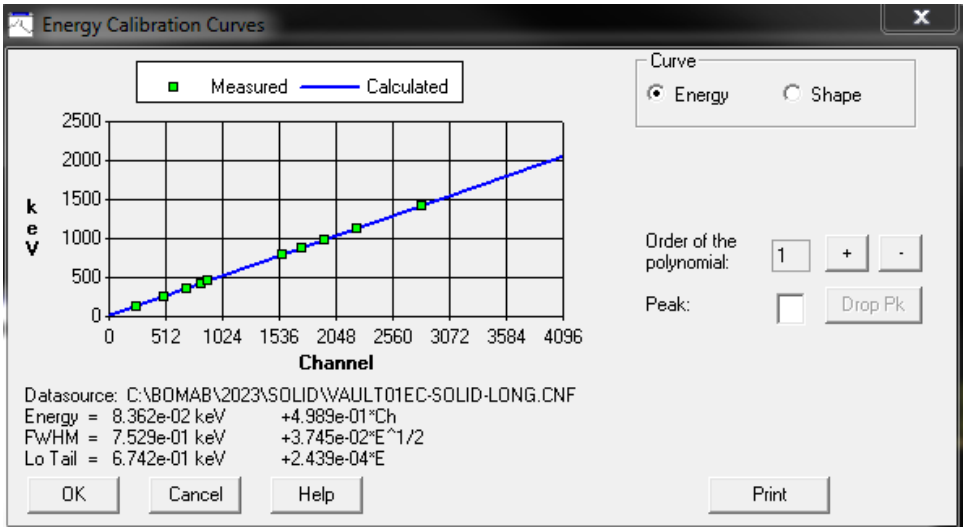

Figure 4.5: V01 energy calibration developed from the solid BOMAB.

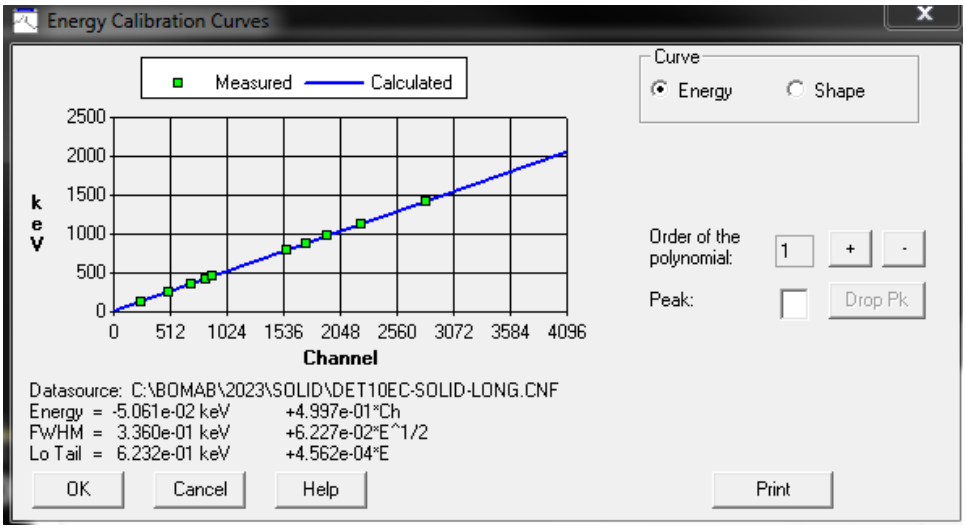

Figure 4.6: DET10 energy calibration developed from the solid BOMAB.

4.3 Performance Testing Verification

The verification results for the performance testing BOMAB, using an empirical curve on V01 can be seen below in Table 24. As shown in the table, the performance testing BOMAB was verified based on the ANSI 13.30 criteria, namely the RMSE being less than 0.25.

Table 24: Performance Testing BOMAB verification using an empirical curve on V01.

Nuclide and Energy (keV)	^{40}K @ 1460.81	^{54}Mn @ 834.83	^{60}Co @ 1173	^{60}Co @ 1332	^{134}Cs @ 604.7	^{134}Cs @ 795	^{137}Cs @ 661.65
Counted Activity	113.00	832.15	884.57	883.61	818.20	767.93	286.75
	109.84	825.96	885.02	889.91	827.27	774.71	287.63
	109.18	826.43	884.70	891.19	830.44	777.08	287.72
	112.08	827.50	889.20	889.46	831.33	783.50	286.89
	113.92	833.27	891.79	891.36	830.77	783.25	287.94
Rounded Average Activity	112	829	887	889	828	777	287
Known Activity	120	857	877	877	862	862	302
Relative Bias Statistic	-0.058	-0.029	0.009	0.008	-0.051	-0.109	-0.05
	-0.085	-0.036	0.009	0.015	-0.040	-0.101	-0.048
	-0.090	-0.036	0.009	0.016	-0.037	-0.099	-0.047
	-0.066	-0.034	0.014	0.014	-0.036	-0.091	-0.05
	-0.051	-0.028	0.017	0.016	-0.036	-0.091	-0.047
Mean Relative Bias	-0.070	-0.033	0.011	0.014	-0.040	-0.098	-0.048
Relative Precision	0.0170	0.0039	0.0037	0.0036	0.0064	0.0075	0.0018
RMSE <= 0.25	**0.072**	**0.033**	**0.012**	**0.014**	**0.010**	**0.099**	**0.048**

*Listed activities are in nCi/tot

The verification results for the performance testing BOMAB, using a cubic spline curve on V01 can be seen below in Table 25. As shown in the table, the performance testing BOMAB was verified based on the ANSI 13.30 criteria, namely the RMSE being less than 0.25.

Table 25: Performance Testing BOMAB verification using a cubic spline curve on V01.

Nuclide and Energy (keV)	**^{40}K @ 1460.81**	**^{54}Mn @ 834.83**	**^{60}Co @ 1173**	**^{60}Co @ 1332**	**^{134}Cs @ 604.7**	**^{134}Cs @ 795**	**^{137}Cs @ 661.65**
Counted Activity	115.52	850.25	874.34	872.84	848.97	787.63	296.98
	112.3	841.15	874.78	879.05	858.36	794.56	296.62
	116.28	831.91	871.86	877.66	856.46	795.99	295.79
	114.59	839.1	878.92	878.62	862.12	793.34	296.68
	115.41	846.22	881.48	880.49	861.7	801.26	296.63
Rounded Average Activity	115	840	880	880	860	795	297
Known Activity	120	857	877	877	862	862	302
Relative Bias Statistic	-0.037	-0.008	-0.003	-0.005	-0.015	-0.086	-0.017
	-0.064	-0.018	-0.003	0.002	-0.004	-0.078	-0.018
	-0.031	-0.029	-0.006	0.001	-0.006	-0.077	-0.021
	-0.045	-0.021	0.002	0.002	0.0001	-0.080	-0.018
	-0.038	-0.013	0.005	0.004	0.0003	-0.070	-0.018
Mean Relative Bias	-0.043	-0.018	-0.001	0.001	-0.005	-0.078	-0.018
Relative Precision	0.013	0.0082	0.0044	0.0033	0.0062	0.0057	0.0015
RMSE <= 0.25	**0.045**	**0.019**	**0.0045**	**0.0034**	**0.0081**	**0.078**	**0.018**

*Listed activities are in nCi/tot

The verification results for the performance testing BOMAB, using an empirical curve on DET10 can be seen below in Table 26. As shown in the table, the performance testing BOMAB was verified based on the ANSI 13.30 criteria, namely the RMSE being less than 0.25.

Table 26: Performance Testing BOMAB verification using an empirical curve on DET10.

Nuclide and Energy (keV)	**^{40}K @ 1460.81**	**^{54}Mn @ 834.83**	**^{60}Co @ 1173**	**^{60}Co @ 1332**	**^{134}Cs @ 604.7**	**^{134}Cs @ 795**	**^{137}Cs @ 661.65**
Counted Activity	114.54	778.14	870.87	868.12	773.76	732.13	269.91
	104.51	787.04	873.05	873.47	770.41	731.14	271.44
	109.83	782.29	868.22	867.27	775.51	728.98	265.88
	111.26	774.8	864.66	859.48	769.53	720.57	265.09
	110.36	773.49	867.96	856.52	765.58	728.90	266.11
Rounded Average Activity	110	780	869	865	770	730	268
Known Activity	120	857	877	877	862	862	302
Relative Bias Statistic	-0.046	-0.092	-0.007	-0.010	-0.102	-0.151	-0.106
	-0.129	-0.082	-0.005	-0.004	-0.106	-0.152	-0.101
	-0.085	-0.087	-0.010	-0.011	-0.100	-0.154	-0.120
	-0.073	-0.096	-0.014	-0.020	-0.107	-0.164	-0.122
	-0.080	-0.097	-0.010	-0.023	-0.112	-0.154	-0.119
Mean Relative Bias	-0.083	-0.091	-0.009	-0.014	-0.106	-0.155	-0.114
Relative Precision	0.0302	0.0065	0.0036	0.0078	0.0045	0.0053	0.0093
RMSE <= 0.25	**0.088**	**0.091**	**0.0099**	**0.016**	**0.106**	**0.155**	**0.114**

*Listed activities in nCi/tot

The verification results for the performance testing BOMAB, using a cubic spline curve on DET10 can be seen below in Table 27. As shown in the table, the performance testing BOMAB was verified based on the ANSI 13.30 criteria, namely the RMSE being less than 0.25.

Table 27: Performance Testing BOMAB verification using a cubic spline curve on DET10.

Nuclide and Energy (keV)	^{40}K @ 1460.81	^{54}Mn @ 834.83	^{60}Co @ 1173	^{60}Co @ 1332	^{134}Cs @ 604.7	^{134}Cs @ 795	^{137}Cs @ 661.65
Counted Activity	120.02	791.50	846.42	846.49	807.38	748.95	280.5
	109.51	800.53	848.55	851.71	803.89	747.94	282.08
	115.09	795.72	843.85	845.66	809.21	745.74	276.31
	116.59	788.10	840.39	838.06	802.98	737.14	275.49
	115.65	786.77	843.59	835.17	798.85	745.66	276.55
Rounded Average Activity	115	790	840	840	800	750	278
Known Activity	120	857	877	877	862	862	302
Relative Bias Statistic	0.000	-0.076	-0.035	-0.035	-0.063	-0.131	-0.071
	-0.087	-0.066	-0.032	-0.029	-0.067	-0.132	-0.066
	-0.041	-0.072	-0.038	-0.036	-0.061	-0.135	-0.085
	-0.028	-0.080	-0.042	-0.044	-0.068	-0.145	-0.088
	-0.036	-0.082	-0.038	-0.048	-0.073	-0.135	-0.084
Mean Relative Bias	-0.039	-0.075	-0.037	-0.038	-0.067	-0.136	-0.079
Relative Precision	0.0316	0.0066	0.0035	0.0076	0.0047	0.0054	0.0097
RMSE <= 0.25	**0.049**	**0.076**	**0.037**	**0.039**	**0.067**	**0.136**	**0.079**

*Listed activities are in nCi/tot

4.4 Hypothesis Testing

First: Solid BOMAB compared to NIST aqueous BOMAB

Alternative: The activity derived from the genie software will not be statistically identical to the calculated spike activity

Null: The activity derived from the genie software will be statistically identical to the calculated spike activity, verifying it as a tissue substitute by comparison

This test was conducted by analyzing the spectra using the energy and interpolated efficiency calibration from a NIST traceable aqueous filled BOMAB filled with the same radionuclide(s). The derived activity was determined to be statistically identical as its value was found to be within two standard deviations of its known value, accepting the null hypothesis and verifying it as a tissue substitute for the specified energy range.

Second: Solid BOMAB compared to DOELAPs Performance Testing BOMABs

Alternative: The calibration curve developed from our fabricated BOMAB will not verify the performance testing BOMAB

Null: The calibration curve developed from our fabricated BOMAB will verify the performance testing BOMAB

This test was conducted by analyzing the spectra of the performance testing BOMAB using the energy and efficiency calibrations from the solid BOMAB. The performance testing BOMAB was verified per the statistical analysis criteria set forth in ANSI 13.30, namely using the mean relative bias and relative precision to calculate the root mean squared error. Accepting the null hypothesis, verifying the use of the tissue substitute as a filler for our calibration standard.

5. SUMMARY AND CONCLUSIONS

5.1 Summary

The goal of the research was to design, fabricate, and verify a BOMAB filled with a solid urethane tissue substitute material thus contributing to the field of radiation protection and dosimetry, advancing the accuracy and reliability of radiation measurements, and enhancing calibrations in diverse environments. The tissue substitute was developed using criteria set forth in ICRU 44 and ICRU 46 and was validated with statistical significance for a broad range of energies. The solid BOMAB was fabricated using guidance and criteria set forth in ANSI 13.35 and the testing of a performance testing BOMAB using the statistical analysis delineated in ANSI 13.30 was affirmatively conducted.

An outcome of this study resolves concerns within the Department of Energy Laboratory Accreditation Program (DOELAP) concerning BOMABs. The aqueous filled BOMABs are prone to leaking and have special shipping requirements relating to their hazards. A solid BOMAB alleviates these concerns by removing the potential risk of shipping acidic aqueous samples.

The findings of this research have implications for improving radiation dosimetry and quality assurance practices, ultimately enhancing the safety and efficacy of various radiological applications. Fulfilling a scientific need, because "a wider range of standard phantoms should be made available and used more regularly" (ICRU 44). "Better tissue substitutes, and fabrication techniques lead to more reliable, realistic phantoms which, together with better computational models, inevitably lead to improved radiation dosimetry and measurement" (ICRU 48).

5.2 Future work

Although this investigation was successful in its endeavor. It can be improved. The addition of more calibration points through the expansion of ^{152}Eu or inclusion of multiple radionuclides will lead to better fitting calibration curves and more precise results. Consistently, additives that can provide more oxygen should be considered as most tissue substitutes are oxygen deficient. Tailoring a calibration phantom to the specific needs of an industry will lead to more trustworthy and defensible work.

The focus of this tissue substitute material in this study was to simulate soft tissue as most human tissue is comprised of this type as well as the significance of using it as a BOMAB filler material. The ease of production and promise of the tissue substitute material indicate that this modifiable material can be used to promote further tissue, organ, and anthropomorphic studies. Furthermore, a solid BOMAB could potentially capture off-gas in long lived natural chains, like radium, creating a calibration source in equilibrium that would outlive generations to come.

6. REFERENCES

Alderson, S. W., Lanzl, L. H., Rollins, M., and Spira, J. (1962). "An instrumented phantom system for analog computation of treatment plans," Am. J. Roentgenol. 87, 185.

ANSI (2011). American National Standards Institute, Performance Criteria for Radiobioassay, Report No. ANSI N13.30 2011 (American National Standards Institute, New York, NY).

ANSI (2022). American National Standards Institute, Specifications for the Bottle Manikin Absorption Phantom, Report No. ANSI N13.35 2022 (American National Standards Institute, New York, NY).

Berger MJ, Hubbell JH, Seltzer SM, Chang J, Coursey JS, Sukumar R, Zucker DS, Olsen K. XCOM: Photon cross sections database. Gaithersburg, MD: US Department of Commerce, National Institute of Standards and Technology; 2020.

Bush F. Energy absorption in radium therapy. British Journal of Radiology 19: 14–21; 1946.

Bush F. The integral dose received from a uniformly distributed radioactive isotope. British Journal of Radiology 22: 96–102; 1949.

Eckerman, K.F., & Cristy, M. (1995). The reference individual of radiation protection (CONF-9507235--1). United States

Delafield HJ. The neutron capture probability for sodium activation in man phantoms. UKAEA, Harwell; AERE-RT128; 1974.

Exempt material activity concentrations and exempt consignment activity limits for radionuclides, 49 C.F.R. § 173.436 (2005)

Fisher, H.L., Snyder, W.S., 1967. Distribution of Dose in the Body from a Source of Gamma Rays Distributed Uniformly in an Organ. ORNL-4168. Oak Ridge National Laboratory, Oak Ridge, TN.

Fryar CD, Gu Q, Ogden CL, Flegal KM. Anthropometric reference data for children and adults: United States. National Center for Health Statistics. Vital Health Stat 3(39): 2011–2014; 2016.

Gama, Nuno V et al. “Polyurethane Foams: Past, Present, and Future.” Materials (Basel, Switzerland) vol. 11,10 1841. 27 Sep. 2018

Genie 2000 3.4 Operations Manual. 2017.

Griffith, R V. Polyurethane as a base for a family of tissue equivalent materials. United States: N. p., 1980. Web.

Hawk, P. B., Oser, B. L., and Summerson, W. H., Practical Physiological Chemistry, The Blakeston Company, Philadelphia, 12th edition, 1947.

Hosea Cheung, Robin S. Tanke, G. Paul Torrence "Acetic Acid" in Ullmann's Encyclopedia of Industrial Chemistry, 2005 Wiley-VCH, Weinheim.

ICRP, 1960. Report of Committee II on Permissible Dose for Internal Radiation. ICRP Publication 2. Pergamon Press, London.

ICRP, 1975. International Commission on Radiation Protection. Report of the Task Group on Reference Man. ICRP Publication 23. Pergamon Press, Oxford.

ICRP, 2009. International Commission on Radiation Protection. Adult Reference Computational Phantoms. ICRP Publication 110. Ann. ICRP 39 (2).

ICRP, 2016. The ICRP computational framework for internal dose assessment for reference adults: specific absorbed fractions. ICRP Publication 133. Ann. ICRP 45(2), 1–74.

ICRU (1964). International Commission on Radiation Units and Measurements, Physical Aspects of Irradiation, ICRU Report 10b, published as National Bureau of Standards Handbook 85 (International Commission on Radiation Units and Measurements, Bethesda, MD).

ICRU (1976). International Commission on Radiation Units and Measurements, Determination of Ab sorbed Dose in a Patient Irradiated by Beams of X or Gamma Rays in Radiotherapy Procedures, ICRU Report 24 (International Commission on Radiation Units and Measurements, Bethesda, MD).

ICRU (1977). International Commission on Radiation Units and Measurements, Neutron Dosimetry for Biology and Medicine, ICRU Report 26 (International Commission on Radiation Units and Measurements, Bethesda, Maryland).

ICRU (1979a). International Commission on Radiation Units and Measurements, Quantitative Concepts and Dosimetry in Radiobiology, ICRU Report 30 (International Commission on Radiation Units and Measurements, Bethesda, MD).

ICRU (1980). International Commission on Radiation Units and Measurements, Radiation Quantities and Units, ICRU Report 33 (International Commission on Radiation Units and Measurements, Bethesda, Maryland).

ICRU (1984b). International Commission on Radiation Units and Measurements, Stopping Powers for Electrons and Positrons, ICRU Report 37 (International Commission on Radiation Units and Measurements, Bethesda, Maryland).

ICRU (1989). International Commission on Radiation Units and Measurements. Tissue Substitutes in Radiation Dosimetry and Measurement, ICRU Report 44 (International Commission on Radiation Units and Measurements, Bethesda, MD).

ICRU (1990). International Commission on Radiation Units and Measurements, Clinical Neutron Dosimetry, ICRU Report 45 (International Commission on Radiation Units and Measurements, Bethesda, Maryland).

ICRU (1992). International Commission on Radiation Units and Measurements. Photon, Electron, Proton and Neutron Interaction Data for Body Tissues, ICRU Report 46 (International Commission on Radiation Units and Measurements, Bethesda, MD).

ICRU (1992). International Commission on Radiation Units and Measurements. Phantoms and Computational Models in Therapy, Diagnosis and Protection, ICRU Report 48 (International Commission on Radiation Units and Measurements, Bethesda, MD).

ISO (2016). International Organization for Standardization, Quality Management and Quality Assurance Standards-General requirements for the competence of reference material producers, Report No. ISO 17034 (International Organization for Standardization, Geneva).

ISO (2017). International Organization for Standardization, Quality Management and Quality Assurance Standards-General requirements for the competence of testing and calibration laboratories, Report No. ISO 17025 (International Organization for Standardization, Geneva).

ISO (2023). International Organization for Standardization, Quality Management and Quality Assurance Standards-General requirements for proficiency testing, Report No. ISO 17043 (International Organization for Standardization, Geneva).

Kienbock, R. (1906). "On the quantimetric method," Arch. Roentgen Ray 11, 17.

LLNL Lawrence Livermore National Laboratory. “Procedure for making Solid BOMAB Phantoms for Whole Body Counter Calibration” 2/1/23

Martin E, James. Physics for Radiation Protection. 3rd Edition. 2013

“Nuclear Data Tables” Labratoire National Henri Becquerel. http://www.lnhb.fr/nuclear-data/nuclear-data-table/

RESL Radiological and Environmental Sciences Laboratory Radiobioassay DOELAP Manual. “Preparing BOMAB Phantoms for Direct Radiobioassay Testing.” 07/14/22.

Sanders FW, Auxier JA. Neutron activation of sodium in anthropomorphous phantoms. Health Physics 8(4): 371–379; 1962.

Schläger, Martin. “Comparison of various anthropomorphic phantom types for in vivo measurements by means of Monte Carlo simulations.” Radiation protection dosimetry vol. 144,1-4 (2011): 384-8.

Spiers, W. (1946). "Effective atomic number and energy absorption in tissues". British Journal of Radiology 19 (52–63): 52–63. doi:10.1259/0007-1285-19-218-52. PMID 21015391.

“The dominant photon interaction based off the energy and atomic number.” Oncology Medical Physics. https://oncologymedicalphysics.com/radiation-interactions/

“The total photon mass attenuation for some material of fixed Z” Oncology Medical Physics. https://oncologymedicalphysics.com/radiation-interactions/

White, D. R, Woodard, H. Q., and Hammond, S. M. (1987). "Average soft tissue and bone models for use in radiation dosimetry," Br. J. Radial. 60,907.

Appendix 1: ANSI 13.30 Minimum Testing Level

Table 28: ANSI 13.30's minimum testing levels for direct radiobioassay.

Measurement category	Type	Radionuclide	MTL [a,b]
I. Transuranium elements via L x-rays	Lung	^{238}Pu	9 kBq (0.24 μCi)
II. ^{241}Am	Lung	^{241}Am	0.1 kBq (2.7 nCi)
III. ^{234}Th	Lung	^{234}Th in equilibrium with its parent ^{238}U	0.5 kBq (14 nCi)
IV. ^{235}U	Lung	^{235}U	30 Bq (0.81 nCi)
V. Fission and activation products	Lung	Any two: ^{54}Mn ^{58}Co ^{60}Co	3 kBq (81 nCi) each
		^{144}Ce or ^{57}Co	30 kBq (0.81 μCi) 3 kBq (81 nCi)
		Plus: ^{134}Cs[c] ^{137}Cs[c]	See footnote c
VI. ^{237}Np	Lung	^{237}Np	30 Bq (0.81 nCi)
VII. Fission and activation products	Total body	All of: ^{134}Cs ^{137}Cs	3 kBq (81 nCi) each
		^{60}Co[c] ^{54}Mn[c]	See footnote c
VIII. Radionuclides in the thyroid	Thyroid	^{131}I and/or ^{125}I	3 kBq (81 nCi)

[a]The upper bound of the testing range shall not exceed 20 times the stated MTL.

[b]The activity of the highest and lowest testing radionuclides (also see footnote c) in any one test phantom shall be within a factor of three of each other except for ^{144}Ce in Category V, whose activity shall not exceed that of any other radionuclide by greater than a factor of 30.

[c]These radionuclides shall be present in the phantom in appropriate amounts for interference but shall not be tested.

Appendix 2: 49 CFR 173.436 Exempt Activity levels

Table 29: Exempt activity levels, per radionuclide, listed in 49 CFR 173.436.

Symbol of radionuclide	Element and atomic number	Activity concentration for exempt material (Bq/g)	Activity concentration for exempt material (Ci/g)	Activity limit for exempt consignment (Bq)	Activity limit for exempt consignment (Ci)
Eu-147	Europium (63)	1.0×10^{2}	2.7×10^{-9}	1.0×10^{6}	2.7×10^{-5}
Eu-148		1.0×10^{1}	2.7×10^{-10}	1.0×10^{6}	2.7×10^{-5}
Eu-149		1.0×10^{2}	2.7×10^{-9}	1.0×10^{7}	2.7×10^{-4}
Eu-150 (short lived)		1.0×10^{3}	2.7×10^{-8}	1.0×10^{6}	2.7×10^{-5}
Eu-150 (long lived)		1.0×10^{1}	2.7×10^{-10}	1.0×10^{6}	2.7×10^{-5}
Eu-152		1.0×10^{1}	2.7×10^{-10}	1.0×10^{6}	2.7×10^{-5}
Eu-152m		1.0×10^{2}	2.7×10^{-9}	1.0×10^{6}	2.7×10^{-5}
Eu-154		1.0×10^{1}	2.7×10^{-10}	1.0×10^{6}	2.7×10^{-5}
Eu-155		1.0×10^{2}	2.7×10^{-9}	1.0×10^{7}	2.7×10^{-4}
Eu-156		1.0×10^{1}	2.7×10^{-10}	1.0×10^{6}	2.7×10^{-5}

Appendix 3: NIST XCOM Without Additive

Table 30: NIST XCOM's calculated attenuation for our tissue substitute without additive compared to the coefficients defined in ANSI 13.35

MeV	keV	Soft Tissue Mass Attenuation Coefficient (m^2/kg)	Tissue Substitute Mass Attenuation Coefficient (m^2/kg)	Acceptance .+/-5%
0.015	15	0.160	0.106	0.663
0.1	100	0.01690	0.01668	0.987
0.2	200	0.01360	0.01352	0.994
0.5	500	0.00960	0.00958	0.998
1	1000	0.00700	0.006994	0.999
1.5	1500	0.00570	0.005692	0.999
2	2000	0.00490	0.004881	0.996
3	3000	0.00393	0.003907	0.994